

1

2 **Dynamics of Snow and Glacier Cover in the Upper Karnali Basin, Nepal: An Analysis of**

3 **Its Relationship with Climatic and Topographic Parameters**

4 **Motilal Ghimire^{1*}, Dibas Shrestha², Raju Chauhan³, Amrit Thapa⁴, Til Prasad Pangali Sharma⁵,**

5 **Krishna Prasad Sharma⁶, Sher Bahadur Gurung⁶, Sundar Devkota⁷, Prabin Bhandari⁸, Sikesh**

6 **Koirala⁷, Yanhong Wu⁹, Niroj Timalsina⁶, and Jeevan Kutu⁶**

7 **¹ Corresponding Author: Tribhuvan University, Central Department of Geography, Kathmandu,**

8 **Nepal. Email: motighimire@gmail.com**

9 **² Tribhuvan University, Central Department of Hydrology and Meteorology, Kathmandu, Nepal**

10 **³ Tribhuvan University, Central Department of Environmental Science, Kathmandu, Nepal**

11 **⁴ University of Alaska Fairbanks, Fairbanks, USA**

12 **⁵ Tribhuvan University, Nepal Mountain Academy, Kathmandu, Nepal**

13 **⁶ Tribhuvan University, Central Department of Geography, Kathmandu, Nepal**

14 **⁷ Department of Survey, Government of Nepal, Kathmandu, Nepal**

15 **⁸ George Mason University, Fairfax, Virginia, USA**

16 **⁹ Institute of Mountain Hazards and Environment, Chinese Academy of Sciences, Chengdu,**

17 **China**

18 **Abstract**

19 Snow and glacier cover in the Upper Karnali Basin (UKB) are crucial freshwater reservoirs that

20 support downstream ecosystems and human populations. This study uses remote sensing and

21 GIS data from various sources, MODIS-derived land surface temperature, and ERA5 reanalysis

22 climate datasets to analyze snow cover dynamics from 2002 to 2024. The results show a

23 significant decrease in snow-covered area (SCA), **with an annual decline of about 3.99 km².**
24 Seasonal variations indicate the most significant reductions during the monsoon period (July–
25 September), **where rising temperatures accelerate snowmelt.** The analysis also establishes a
26 **strong negative correlation between snow cover and temperature ($r = -0.59$ to -0.77 , $p <$**
27 **0.05)**, with warming trends disproportionately affecting mid-to-high elevation zones (3000–5000
28 m a.s.l.). Glacier basins exhibit consistent retreat, **with the mean glacier area declining from**
29 **119.05 hectares in 2000 to 100.47 hectares in 2023**, highlighting the impact of climate change.
30 Additionally, **snowline analysis demonstrates an upward migration, with the 10th percentile**
31 **snowline increasing at a rate of approximately 5.16 m/year**, which indicates progressive snow
32 loss at lower elevations. **Given the current warming trends (~0.0643°C/year above 5000 m**
33 **a.s.l.), the UKB could experience a decline of glacier area by 47–69 % and snow-covered**
34 **area by 19–30 %.** These findings emphasize the vulnerability of UKB's cryosphere to climate
35 change, necessitating adaptive water resource management strategies. **This will help mitigate**
36 **impacts on hydrology, agriculture, and regional water security.**

37 **Keywords:** Snow and Glacier, Karnali, Himalayas, Remote Sensing, Climate Change,
38 Elevation-depended-warming, Snowline

39

40 **1. Introduction**

41 Snow and glaciers in the mountains act as freshwater towers. Their meltwater provides a
42 consistent supply to rivers and downstream ecosystems (Immerzeel et al., 2020; Wester et al.,
43 2019; Pritchard, 2019). The meltwater from Himalayan ice and snow supports the livelihoods of
44 millions across Nepal, India, and China by supplying drinking water, irrigation, hydropower, and
45 ecosystem services (Bolch, 2007; Bookhagen and Burbank, 2010). Therefore, a decline in snow
46 and glacier extent threatens water availability, food security, and sustainable development in
47 these regions (Krishnan et al., 2019).

48 Furthermore, snow and glacial ice regulate regional and global climates by reflecting solar
49 radiation, thereby contributing to the Earth's energy balance and influencing local weather
50 patterns (Xu et al., 2009). Seasonal meltwater sustains ecosystems that provide habitats for
51 numerous animal and plant species in mountainous regions. Consequently, changes in snow
52 cover and glaciers can disrupt these entirely (Wester et al., 2019). On both local and regional
53 scales, variations in the amount of snow and ice can contribute to changes in sea level, affecting
54 coastal areas (Forster et al., 2021; Mimura, 2013; NOAA, 2013)

55 **Snow-covered peaks and glaciers are major hubs for adventure, religious, and nature-**
56 **based tourism** (Anup, 2017; Nyaupane and Chhetri, 2009). **Being sensitive to climate change,**
57 **changes in their size and volume not only serve as visible indicators of broader climate**
58 **trends but also directly threaten the tourism economy they support** (Elsasser and Bürki,
59 2002).

60 A comprehensive understanding of cryospheric transformations is essential for accurate
61 hydrological forecasting, assessing cryospheric hazards, and developing effective adaptation

62 strategies. Historically, monitoring snow and glacier dynamics in the remote Himalayan regions
63 was limited by a scarcity of in-situ observations. Since the 1970s, advances in satellite remote
64 sensing have revolutionized large-scale cryospheric assessments (Kääb et al., 2012; Muhammad
65 and Thapa, 2020). The synergistic integration of satellite-derived data with sophisticated climate
66 models and targeted ground-based measurements has subsequently enabled improved
67 understanding of snow and glacier mass balance changes, their resultant hydrological impacts,
68 and spatiotemporal variability (Bajracharya et al., 2014; Bolch et al., 2012; Gurung et al., 2017;
69 Kääb et al., 2012; Krishnan et al., 2019; Kulkarni et al., 2021). **Collectively, these studies**
70 **demonstrate substantial snow and glacier loss across the Himalayas, altering river**
71 **discharge seasonality and water resource availability**

72 Extensive research on glaciers, glacier lakes, and glacier lake outburst floods (GLOFs) in Nepal
73 has been conducted (Bajracharya et al., 2008; Hall et al., 2002; Kääb et al., 2005; Shrestha et al.,
74 2012; Zemp, 2006). However, these studies disproportionately focus on the central and eastern
75 Himalayas. **The mid-western and far-western regions remain underrepresented due to their**
76 **remoteness and limited accessibility** (Shrestha et al., 2019; Khadka et al., 2024). Although
77 global and regional glacier inventories specifically addressing high-resolution (≤ 30 m) glacier
78 cover remain limited (Bajracharya et al., 2014; Bolch et al., **Analyses of elevation-dependent**
79 **warming (EDW) and trend analyses are also scarce in the Himalayas** (Pepin et al., 2015;
80 Pepin et al., 2022; Desinayak et al., 2022). **Furthermore, integrated studies linking glaciers,**
81 **glacier basins, and snow cover to climate remain underexplored.**

82 **Bridging this gap is crucial for understanding cryosphere dynamics and their impacts on**
83 **hydrology, hazards, and livelihoods in western Nepal.** The Karnali Basin, Nepal's largest
84 river basin ($\sim 40,780$ km 2 upstream of the Chisapani gauge station) **and home to approximately**

85 **2.5 million people** (CBS, 2021), exemplifies this need. Its rivers, fed by snow, **provide essential**
86 **dry-season water for irrigation, drinking, and hydropower. Despite its ecological**
87 **significance, the basin's cryospheric behavior remains poorly documented.**

88 **Findings from studies conducted in the central and eastern Himalayas, the Indian**
89 **Himalayas, and the Tibetan Plateau cannot be universally applied to the Karnali Basin due**
90 **to differences in climatic regimes and geographical settings.** Understanding the impacts of
91 cryosphere changes on water resources requires studies specific to the Karnali Basin.
92 **Integrating MODIS data, which offers high temporal resolution, with Landsat data, known**
93 **for high spatial resolution, will improve our understanding of snow and glacier changes** and
94 their relationships with topography, glacier basins, and climate.

95 **Against this backdrop, the specific objectives of these study are to:**

96 **1. Quantify spatial and temporal variations in snow and glacier cover in the Upper**
97 **Karnali Basin (2000–2024) using multi-sensor remote-sensing datasets.**
98 **2. To determine the influence of climatic drivers (rising temperatures, precipitation**
99 **shifts) and topography on the observed cryospheric dynamics, including the upward**
100 **migration of the snowline.**

101 **2. Study Area**

102 The Upper Karnali Basin (UKB) is a transboundary catchment extending from 28.64° to 30.68° N latitude
103 and 80.64° to 83.54° E longitude, covering 22,577 km². This region accounts for over 50% of the entire
104 Karnali Basin above the Chisapani gauge station (225 m above sea level). It includes about **66% of the**
105 **basin's glacierized area** (Bajracharya et al., 2011; Ghimire et al., 2024). The UKB comprises the Humla
106 Karnali (partly within Tibet, China), Mugu Karnali, Kawari, and Tila Nadi sub-basins (see Fig. 1).

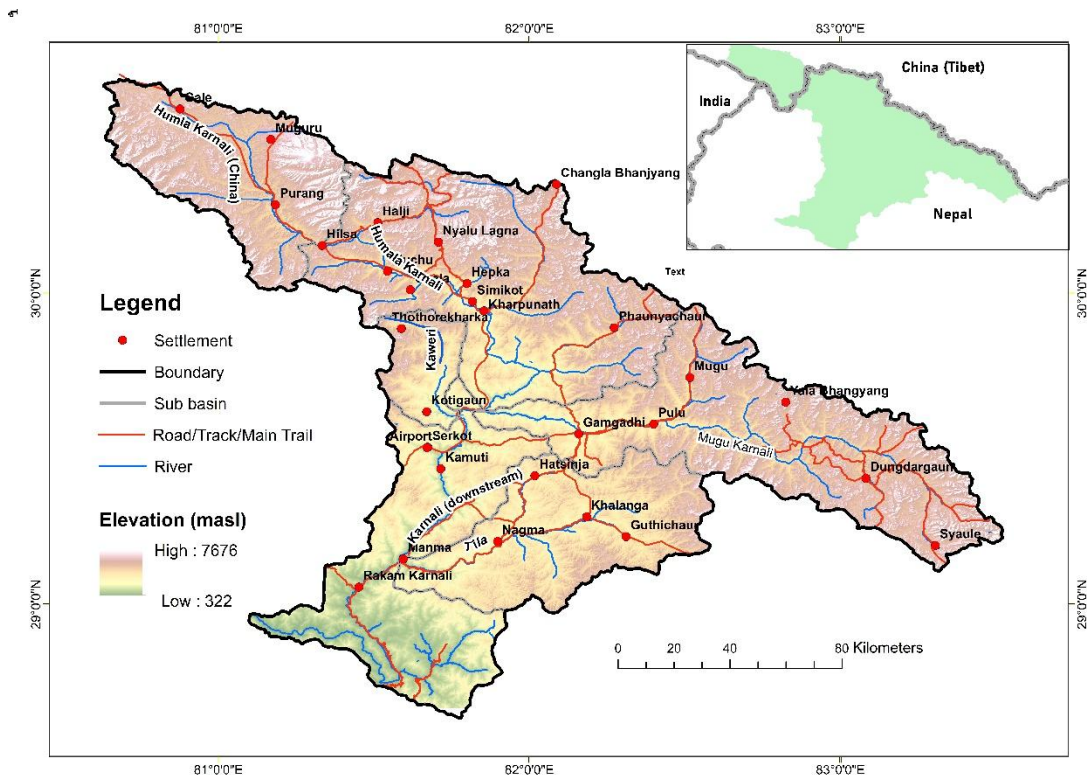
107 The Upper Karnali Basin (UKB) **is a transboundary catchment** extending from 28.64° to
108 30.68° N latitude and 80.64° to 83.54° E longitude, covering 22,577 km². **This region accounts**
109 **for over 50% of the entire Karnali Basin above the Chisapani gauge station (225 m above**
110 **sea level). It includes about 66% of the basin's glacierized area (Bajracharya et al., 2011;**
111 **Ghimire et al., 2024).** The UKB comprises the Humla Karnali (**partly within Tibet, China**),
112 Mugu Karnali, Kawari, and Tila Nadi sub-basins (see Fig. 1).

113 The elevation ranges from 340 meters to 7,030 meters, with an alpine zone above 4,000 meters
114 extending across the Middle Mountains, High Mountains, High Himalaya, and the Tibetan
115 Plateau. **These regions encompass the geological units known as the Lesser Himalaya,**
116 **Higher Himalaya, and Tethys Himalaya (LRMP 1986; Dhital 2015).** This topographic and
117 **lithologic diversity significantly influences climatic gradients and cryospheric processes.**

118 The climate ranges from polar tundra in the glacier region to subtropical, temperate, and cold
119 climates below 4,000 meters, with mean annual temperatures ranging from 27 °C to -12 °C and
120 precipitation varying from **250 mm in rain-shadow areas to approximately 1,900 mm**
121 annually on slopes. The cryosphere spans across both rainy and rain-shadow areas, which
122 influences the distribution and mass balance of snow and glaciers.

123 The Upper Karnali Basin features a diverse landscape of snow-covered glaciers, valleys,
124 permafrost, alpine meadows, and forests, supporting a rich variety of flora and fauna. It
125 represents a cultural blend of Khas and Tibetan traditions and is an emerging tourist destination,
126 including a stop on the Kailash Mansarovar pilgrimage route. The basin has an estimated
127 population of approximately 816,941 people, with a density of 36.2 persons per square
128 kilometer, residing in 4,395 settlements, primarily below 4,000 meters in elevation. The Human
129 Development Index in the area is 0.49, which is below the national average.

130 Due to its climatic, geological, and cryospheric diversity, the Upper Karnali Basin
131 represents the broader Himalayan environment. It serves as an ideal natural laboratory for
132 studying spatial variations in snow- and glacier-covered areas, elevation-dependent
133 warming, and hydro-cryospheric changes across far and mid-western Nepal.



134

135 **Figure 1.** Location of the Upper Karnali Basin.

136

137 **3. Data Sources, Method, and Limitations**

138 This study considers snow and glacier cover as a unified cryospheric component, given
139 their analogous functional roles. This study analyzed cryospheric dynamics using remote
140 sensing. Satellite imagery was processed to generate time-series data on snow and ice cover,
141 derive land-surface temperatures, and map glacier basins.

143

144 **3.1.Snow Cover Mapping**

145 We mapped snow cover in the Upper Karnali Basin using Google Earth Engine (GEE) and
146 imagery from Landsat 5 TM, Landsat 7 ETM+, and Landsat 8 OLI. For the period
147 preceding the Scan Line Corrector (SLC) failure, we used only Landsat 7 ETM+ images
148 (2002–2003). For subsequent years, we utilized data from Landsat 5 TM and Landsat 8
149 OLI. To ensure high data quality, we selected only scenes with less than 30% cloud cover
150 (Appendix A)

151 We preprocessed all Landsat images by masking clouds using the Quality Assessment (QA)
152 bands–pixel_qa for Landsat 5 and 7, and QA_PIXEL for Landsat 8. Next, we calculated the
153 Normalized Difference Snow Index (NDSI) using the green and short-wave infrared (SWIR)
154 bands (Hall et al., 2002; Gorelick et al., 2017) and applied a threshold of NDSI > 0.4 to identify
155 snow pixels. To reduce confusion between snow and vegetation in mixed or forested terrain,
156 we also calculated the Normalized Difference Vegetation Index (NDVI) and excluded pixels
157 with NDVI > 0.2 from the snow classification, following the approach of Rittger et al.
158 (2013). Finally, we exported the resulting snow cover maps as GeoTIFF files for overlay
159 and sub basin and micro-basin analyses.

160 To supplement the Landsat observations, we processed MODIS 8-day composite snow-
161 cover products (MOD10A2) using Google Earth Engine (GEE). The MOD10A2 algorithm
162 applies a maximum snow-extent compositing method over each 8-day period (Parajka and
163 Blöschl, 2008), which minimizes cloud contamination and produces a spatially continuous
164 dataset for analyzing seasonal and interannual snow-cover variability. Although it loses

165 **daily temporal resolution, the 8-day composite effectively smooths out short-lived cloud**
166 **effects, providing a more stable dataset for trend analysis.**

167 **After processing the imagery, we executed a Python script within the Google Earth Engine**
168 **(GEE) environment to automate the download and organization of snow cover data. The**
169 **script aggregated MODIS-derived snow extent by season, sub-basin, and elevation band**
170 **(derived from the SRTM DEM).**

171 **The year was divided into four distinct three-month periods—January–March (Peak**
172 **Accumulation), April–June (Major Ablation), July–September (Monsoon Ablation), and**
173 **October–December (Early Accumulation). This division was explicitly chosen to capture**
174 **the hydrological phases of snow accumulation and melting while minimizing cloud**
175 **contamination during the monsoon season(Hunt et al., 2025; Khatiwada et al., 2016;**
176 **Kulkarni et al., 2017). The resulting structured snow dataset was used as the main input**
177 **for analyzing snow cover trends, elevation-dependent variability, and hydrological**
178 **differences among sub-basins.**

179 **We describe the methods for spatial resolution harmonization and accuracy assessment**
180 **between Landsat and MODIS datasets in Appendix B. Despite these refinements, persistent**
181 **monsoon cloud cover continues to limit optical remote sensing in the Himalayas, often**
182 **resulting in underestimation of snow-covered areas and uncertainties in seasonal trends.**

183 Elevation bands were defined using the SRTM DEM and categorized into 200-meter intervals,
184 ranging from ≤ 2000 m to ≥ 6500 m. Zonal statistics were applied to extract the frequency of
185 snow cover for each elevation band and subbasin. Snow-covered area was calculated using a
186 threshold-based binary mask. The results were aggregated into a structured dataset, revealing

187 seasonal snow distribution and variations across elevation zones and watersheds, thereby
188 facilitating hydrological analysis.

189 **3.2. Land Surface Temperature Data and Validation**

190 **We also downloaded the land surface temperature (LST) 1 km resolution from the**
191 **Application for Extracting and Exploring Analysis Ready Sample (AppEEARS) platform.**
192 **AppEEARS is a NASA-supported platform developed to easily access, subset into specified**
193 **areas, and analyze climate and environmental data(Wan et al., 2015). MODIS Land**
194 **Surface Temperature (LST) data have been reliably used to determine surface temperature**
195 **patterns in areas where ground observations are scarce, especially in rugged mountainous**
196 **regions. Several studies have confirmed their accuracy, showing average biases of less than**
197 **1.5 K and high correlations ($R^2 > 0.9$) with on-site measurements (Duan et al., 2019; Yu et**
198 **al., 2011; Zhao et al., 2019), demonstrating their appropriateness for analyzing elevation-**
199 **related warming trends in the Himalayas. We also obtained temperature and precipitation**
200 **records, including maximum and minimum values, from the Department of Hydrology and**
201 **Meteorology (DHM), Government of Nepal, and open-access reanalysis datasets such as**
202 **ERA5. The temperature data (2 m above ground) obtained from various meteorological**
203 **stations in the study area, were compared with MODIS LST; the results of this**
204 **comparison are discussed in Section 4. Due to the 1 km spatial resolution of the MODIS**
205 **product, the analysis of time series data reflects area-averaged temperature trends rather**
206 **than in situ measurements at individual stations.**

207 **3.3. Delineation of the Glacier Basin and Glacier Data**

208 The boundaries of glacier basins were **delineated to assess changes in glaciers and snow cover**
209 **fractions within glacier-drained areas. Glacier basins include trunk glaciers, tributary**
210 **glaciers, and surrounding slopes nourished by moving ice and snow. Their boundaries are**
211 **topographically defined, with the lower boundary terminating at the terminus of the main**
212 **glacier. This delineation process involved multiple steps to ensure accuracy.**

213 Initially, the Glacier Inventory map referenced earlier served as a fundamental resource. High-
214 resolution imagery and ESRI's topographic maps in ArcGIS 10+ and later versions provided
215 detailed spatial data. A 12.5 meter DEM was used to extract drainage networks, produce contour
216 lines, and generate hillshade maps, enhancing the visualization of divides between glacier basins.
217 **These components were essential for accurately identifying glacier termini and delineating**
218 **glacier head basins. This integrated approach**, combining topographic analysis, remote
219 sensing, and geospatial techniques, enabled precise delineation of glacier basins for
220 comprehensive evaluations of snow cover fraction.

221 The time series glacier data compiled by Ghimire et al. (2025), were included in this study. The
222 lead author of the current manuscript was also responsible for that research paper. In summary,
223 we mapped glacier polygons for the years 2000, 2010, and 2023 using high-resolution imagery
224 from Google Earth, Bing Maps, and RapidEye 2023 to maintain temporal consistency. Snow and
225 glaciers were identified based on their bright characteristics, features, smooth textures, and
226 shadows cast by adjacent terrain. Landsat composites (both true and false color) and the
227 Normalized Difference Snow Index (NDSI) enhanced and improved the visibility of snow and
228 ice, while altitude and topographic data derived DEM highlighted potential glacier regions.
229 Outlines from the Randolph Glacier (RGI)(Pfeffer et al., 2014) and ICIMOD (Bajracharya et al.)

230 served as reference, while ground-truth and additional data helped validate the findings. This
231 comprehensive approach ensured precise delineation.

232 **3.4.Limitations and Validation**

233 **A key limitation of this research is that optical remote sensing is significantly affected by**
234 **cloud cover, particularly during the monsoon season (Hall et al., 2002; Gafurov and**
235 **Bárdossy, 2009). Frequent cloudiness often restricts the availability of clear Landsat**
236 **images, leading to an underestimation of snow cover and potential inaccuracies in the**
237 **spatial and seasonal assessment of snow patterns. In this study, cloud-free images were**
238 **primarily available from January to March and October to December in most Upper**
239 **Karnali sub-basins. Nevertheless, all four seasons were analyzed for microglacier basins where**
240 **suitable data existed.**

241 To address these issues, we used MODIS MOD10A2 data, **which provide higher temporal**
242 **resolution (8-day composites at 500 m) compared to Landsat's 16-day revisit cycle and 30**
243 **m spatial resolution. This multi-sensor strategy enhances temporal continuity and**
244 **minimizes data gaps caused by clouds; however, results should still be interpreted**
245 **cautiously (Maskey et al., 2011; Parajka and Blöschl, 2008).**

246 **The scarcity of high-altitude temperature stations necessitated the use of MODIS land**
247 **surface temperature (LST) data at a 1 km resolution, representing daytime skin**
248 **temperature at approximately 10:30 A.M. local time. This skin temperature was compared**
249 **with in situ air temperature measurements taken at 2 meters above ground from four**
250 **stations: Jumla (2,300 m), Simkot (2,800 m), Guthi Chaur (3,080 m), and Rara (3,048 m).**
251 **Correlations varied by site and season—strongest at Jumla (up to 0.85), moderate at Guthi**
252 **Chaur, and weakest at high-altitude, snow-covered sites such as Simkot and Rara (−0.18).**

253 **MODIS LST performs well in clear, snow-free areas but requires adjustments at higher**
254 **elevations. Differences arise from factors including resolution, spatial averaging, land-**
255 **cover heterogeneity, and surface–air temperature contrasts.**
256 **Validation studies further confirm its reliability for analyzing high-mountain temperatures**
257 **in regions where in situ data are limited (see Duan et al., 2019; Yu et al., 2011; Zhao et al.,**
258 **2019).**

259 **4. Result**

260 **4.1. Snow or Ice cover Trend and Variability: Annual and Seasonal**

261 The total snow cover across the Upper Karnali Basin (22,546 km²) from 2002–2024 averages
262 872 km², with a standard deviation of 147 km², indicating moderate variability (Table 1 and
263 Figure 2). The minimum recorded snow cover is 514 km²; about 25% of the recorded snow
264 cover observations are at or below 777 km². The average snow covered area from January–
265 March is 1528 ± 333 km², followed by April–June (881 ± 212 km²) and October–December
266 (862 ± 373 km²), respectively. July–September witnessed the lowest snow cover area, i.e., 169
267 ± 38.3 km².

268 Snow cover data highlight significant year-to-year changes in every quarterly season with
269 varying directions and magnitudes of trends, evidenced by correlation, the Kendall tau test, and
270 Sen's slope. The annual average SCA shows, although not significant, a decreasing trend ($p =$
271 0.535), with Sen's Slope estimating a loss of ~ 3.99 km²/year, which indicates a gradual decline in
272 snowpack over two decades. Seasonally, the July–September period exhibits a gentler trend line
273 compared to October–December; however, because of its much lower inter-annual variability, this
274 period exhibits the statistically significant steepest drop in snow cover (Sen's Slope = -2.87, $p =$
275 **0.001**) (**Table 1**). This period is charactersied by snow ablation, where the summer monsoon

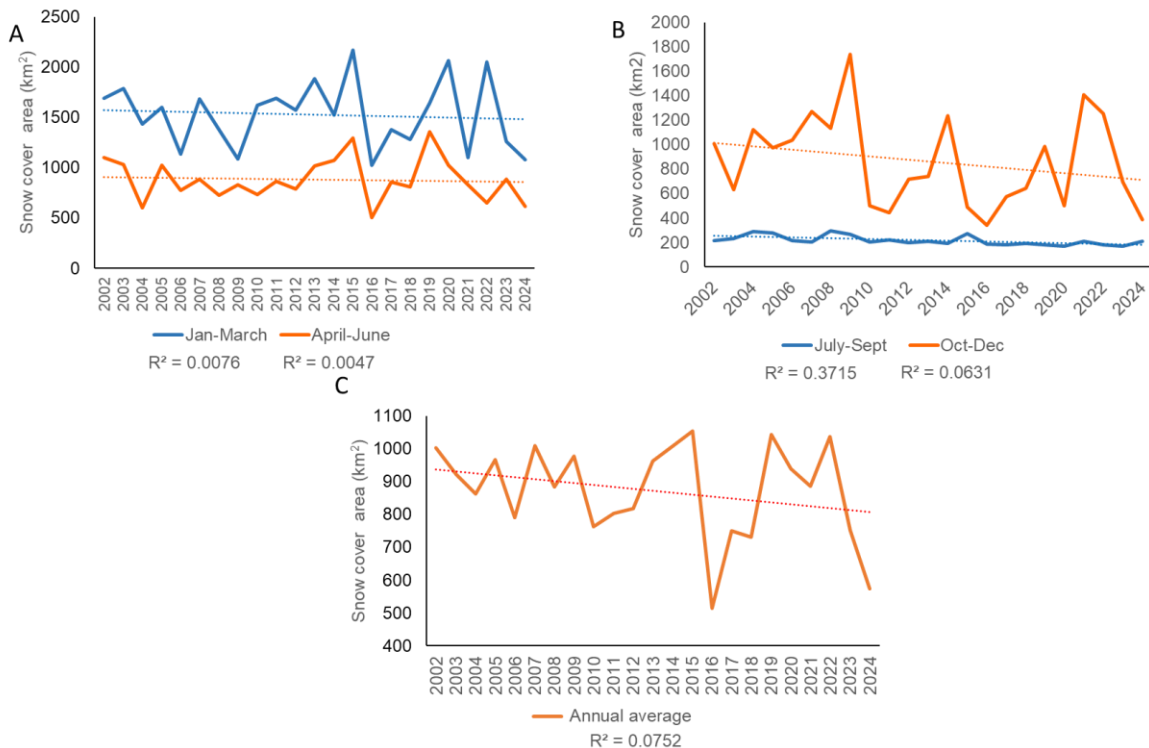
276 brings warmer temperatures. In mid-latitude regions, the precipitation occurs more as rain than
277 snow, resulting in accelerated snowmelt. While January–March shows a decline (Sen's slope =
278 8.63 km/year), it lacks statistical significance ($p = 0.523$), suggesting year-to-year winter
279 variability in snowfall or early melt. Similarly, no significant trends were detected in April–June.
280 Interannual variability is evident with peaks and lows of snow and ice coverage (Figure 2).
281 Episodic snow coverage was observed in 2015, 2020, and 2022 (January–March), 2015 and 2019
282 (April–June), 2009, and 2021 (October–December), **indicating anomalous years of high**
283 **episodic** heavy snowfall events. However, these anomalies do not counterbalance long-term
284 declines. Compared to seasons, annual snow coverage's inter-annual variability is relatively low,
285 i.e., with a 16% coefficient of variation (CoV)–ratio of the standard deviation to the mean.
286

287

288 **Table 1.** Snow cover descriptors and changes by seasons

Descriptor	Jan–Mar	Apr–Jun	Jul–Sep	Oct–Dec	Annual avg.
Mean (km ²)	1 528.00	881.00	217.00	862.00	872.00
Median (km ²)	1 569.00	858.00	210.00	739.00	886.00
Std. dev. (km ²)	333.00	212.00	38.30	373.00	147.00
Minimum (km ²)	1 025.00	503.00	169.00	340.00	514.00
Maximum (km ²)	2 167.00	1 358.00	298.00	1 737.00	1 055.00
Skewness	0.21	0.47	0.94	0.51	-0.87
25th percentile (km ²)	1 270.00	751.00	191.00	538.00	777.00
50th percentile (km ²)	1 569.00	858.00	210.00	739.00	886.00
75th percentile (km ²)	1 689.00	1 025.00	229.00	1 126.00	991.00
Correlation (r)	-0.09	-0.07	-0.61	-0.25	-0.27
Kendall's τ	-0.09	0.01	-0.54	-0.13	-0.10
p-value	0.523	0.950	0.000	0.398	0.535
Sen's slope (km ² yr ⁻¹)	-8.63	-3.14	-2.87	-13.21	-3.99

289 **Note:** Sen's slope represents the median of all possible pairwise slopes, quantifying trend (here
 290 snow cover) over time (Sen, 1968). It gives a more reliable long-term trend of snow cover loss
 291 without being skewed by short-term anomalies (Gilbert, 1987; Yue and Wang, 2004)



292

293

294 **Figure 2.** Temporal variation and trends in seasonal and annual snow-covered area (SCA) in the
 295 Upper Karnali Basin (2002–2024).a) Time series of SCA for January–March (orange) and April–
 296 June (orange); (b) SCA for July–September (blue) and October–December (orange); (c) average
 297 annual SCA (orange).

298 **4.2. The Relation among Snow Cover, Temperature, and Precipitation**

299 We derived land surface temperature (LST) data for 204 locations from MODIS Terra
 300 (MOD11A1) and Aqua (MYD11A2) (1 km resolution), which were processed through
 301 AppEEARS. Precipitation data were obtained from the ERA5-Land reanalysis (~9 km
 302 resolution) by ECMWF (Hersbach et al., 2020). These datasets, covering four different
 303 seasons, were used to examine temperature and precipitation trends, as well as their
 304 relationship with snow cover trends (Figures 3, 4, and 5).

305

306 Using correlation statistics, we found that among the 204 sampled sites, 143 locations
307 (approximately 70%) exhibit a positive annual temperature trend, indicating a general warming
308 pattern throughout the study region (Figure 3). However, statistically significant trends ($p \leq 0.1$)
309 were identified in only a subset of these sites, highlighting that not all observed warming trends
310 are statistically robust. Moreover, the warming pattern is not consistent across all seasons.
311 Notably, during the April–June interval, the temperature trend tends to be weaker or, in some
312 cases, negative. Several subsites across different seasons also demonstrate negative trends,
313 although the majority of locations show a positive trend (Figure 3). Elevation-related variability
314 in these trends is further analyzed in Figures 7–9 and Table 3.

315 **Seasonal rainfall trends from 2000 to 2024 indicate weak to moderate increases across all**
316 **seasons, with the exception of winter (January–March), which exhibits a slight downward**
317 **trend ($R^2 = 0.0144$) (Figure 4). Pre-monsoon (April–June) rainfall shows a slight upward**
318 **trend ($R^2 = 0.0119$). All these seasons display high variability, suggesting a limited impact**
319 **on snow accumulation. Monsoon rainfall (July–September) demonstrates a more noticeable**
320 **increase ($R^2 = 0.0975$), primarily contributing to rainfall rather than snowfall. Post-**
321 **monsoon (October–December) precipitation remains low and stable. When combined with**
322 **rising temperatures, these trends indicate a shift toward rainfall-dominated precipitation,**
323 **reduced snowfall, and earlier snowmelt, contributing to declining snow cover and altered**
324 **hydrological regimes.**

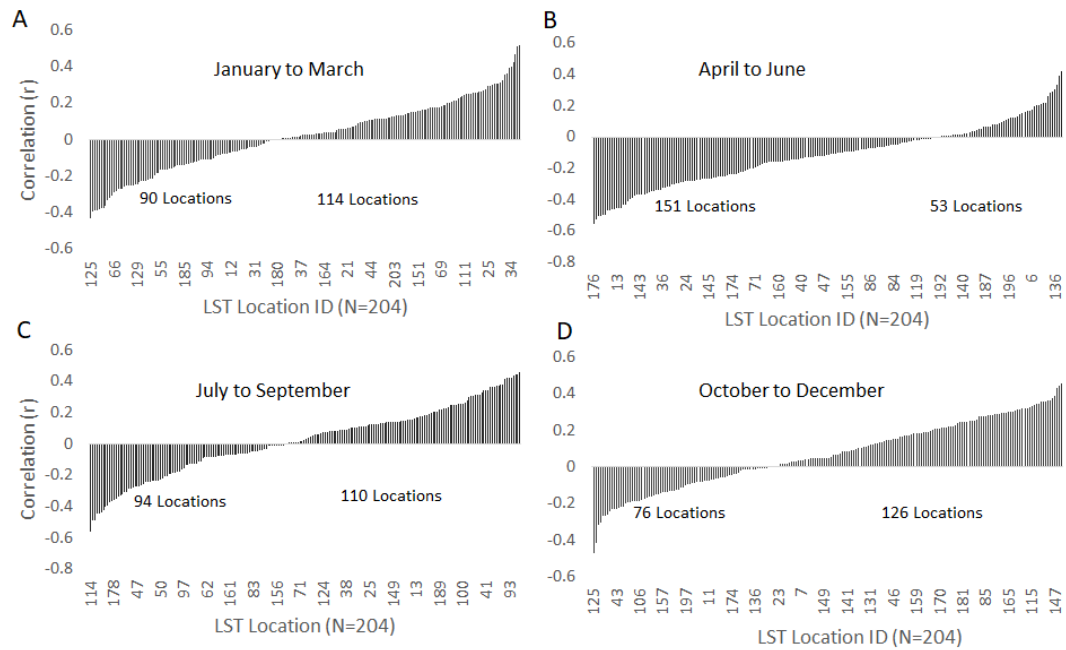
325 The snow-covered area shows a strong to moderate negative correlation ($r = -0.59$ to -0.77 , $p <$
326 0.05) with temperature across all seasons (Figure 5). Conversely, precipitation has a positive
327 correlation ($r = 0.55$ to 0.59 , $p < 0.05$) with snow cover for January–March and October–

328 December, while during the remaining seasons, it shows a moderate negative correlation.

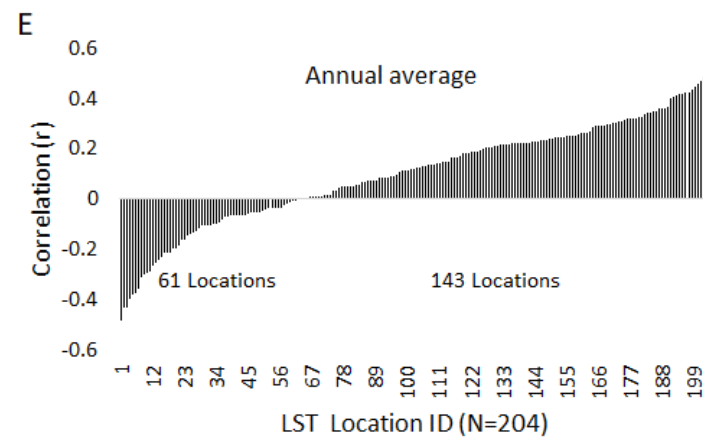
329 **Precipitation and temperature are negatively correlated in winter (Oct-March) and**
330 **positively in the summer (April-September) half-year.**

331

332



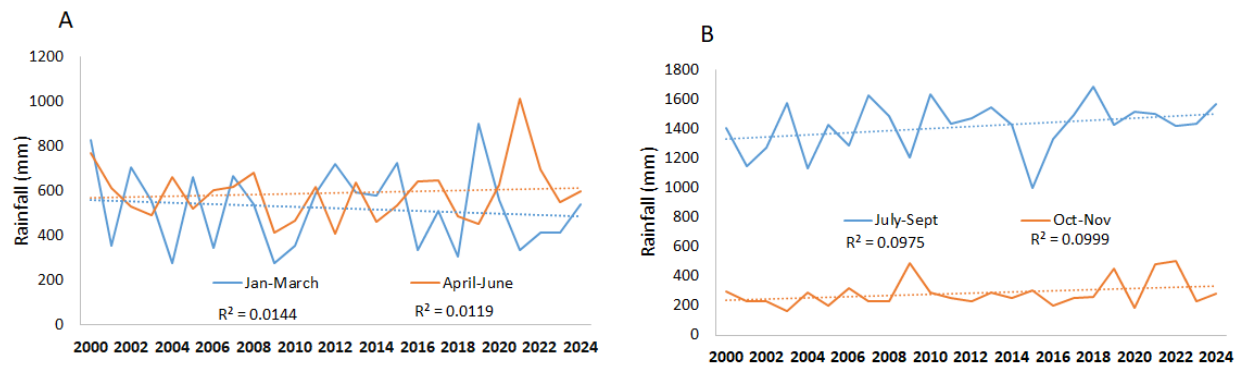
333



334

335 **Figure 3.** The correlation illustrates the season wise (A-E) temperature trend directions at
336 various sites between 2000 and 2024 (Source: MODIS Terra and Aqua MOD11A2, MYD11A1,
337 AppEEARS). Significant correlations at a 90 % confidence level are observed at $r = \pm 0.364$.

338

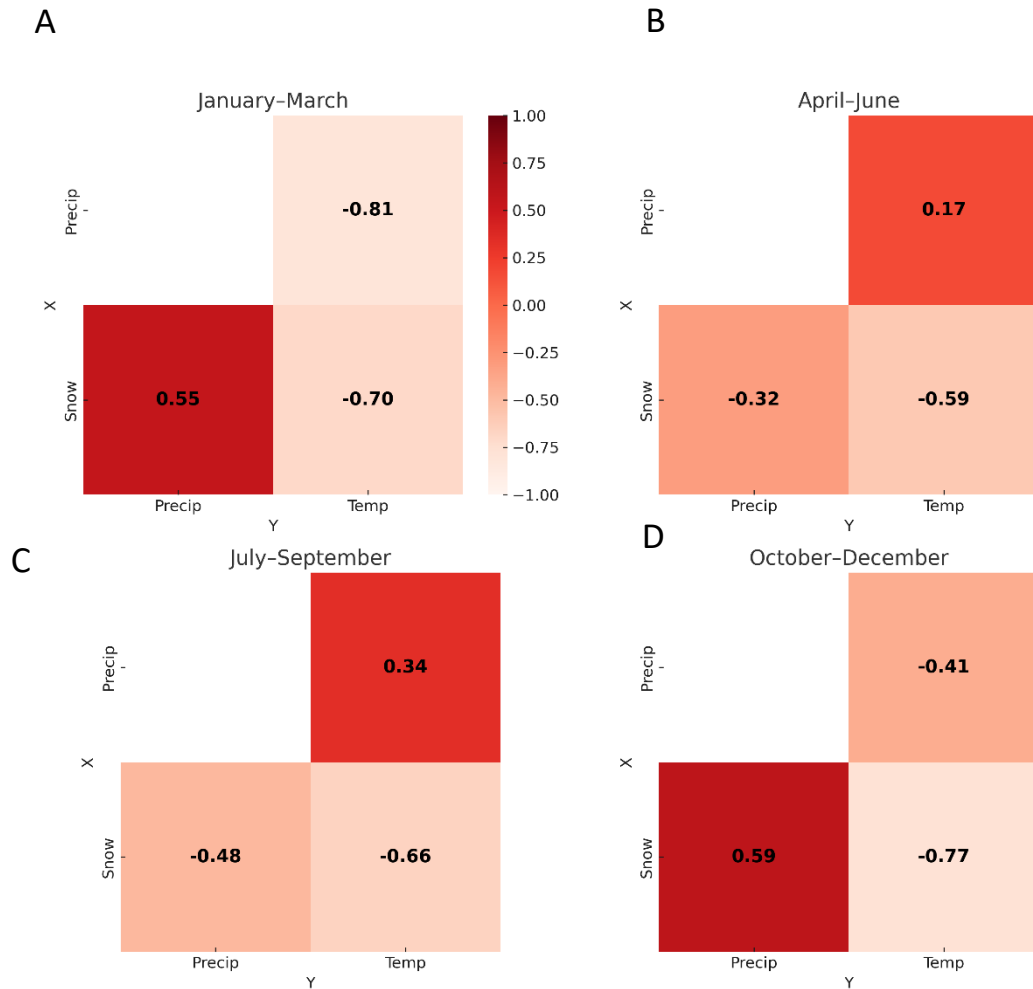


339

340

341 **Figure 4.** Yearly rainfall trends across various periods. Precipitation data was collected from the
342 ERA5-Land reanalysis by ECMWF (Hersbach et al., 2020) from 204 locations across four
343 different periods.

344



345

346 **Figure 5.** Seasonal correlation patterns among snow cover, temperature, and precipitation across
 347 a 22-year period, shown separately for each season (A–D).

348 **4.3. Snow Cover Changes in Sub-Basins Using Landsat Series Data**

349 Landsat-derived reliable snow and ice data were unavailable for the pre-monsoon and monsoon
 350 seasons due to significant cloud coverage (as mentioned in Section 3.4). Therefore, only two
 351 seasons, January–March and October–December, were considered. These seasons are
 352 characterized by snowfall as precipitation, which contributes to snow accumulation.

353 Examining snow cover patterns in the sub-basins of the Upper Karnali Basin (UKB) for two
 354 seasons (January–March and October–December) reveals notable seasonal and spatial

355 differences (Table 2). During January–March, Humla Karnali has the largest average snow cover
356 (3,336 km²), followed by Mugu Karnali (1,864 km²) **and Humla Karnali (China)** (1,478 km²),
357 while areas downstream like Tila and Kawari have very little coverage (less than 350 km²).
358 Significant variability in the snow cover trend is observed, particularly in Tila and Downstream
359 Karnali, which have a coefficient of **variation (CoV) above 50%. This high CoV indicates**
360 **inconsistent snow cover from year to year during January–March. Furthermore, this**
361 **variability is associated with a significant negative correlation i.e., $r \geq -0.37$ ($p < 0.1$). Figure**
362 **6 also graphically shows the temporal trends with the correlation coefficient (r) and**
363 **fluctuations in Landsat-derived snow cover for the two seasons mentioned above.** The
364 **moderately negative skewness of the temporal distribution does not affect the correlation, which**
365 is negative for all basins, indicating a declining trend.

366 Conversely, the October–December season has a lower average snow cover (823 km²) and
367 exhibits strong fluctuations (e.g., a range of 227–1570 km² and a CoV of 55%). Strong
368 variability is observed for all basins, particularly Humla Karnali (China), Tila, and Downstream
369 Karnali. The skewness is moderate, except for Downstream Karnali. Correlation values are
370 reliable and indicate a declining trend. However, Downstream Karnali, in spite of high
371 variability, indicates a statistically significant negative r value, i.e., -0.47 ($p < 0.05$) (Figure 6).

372

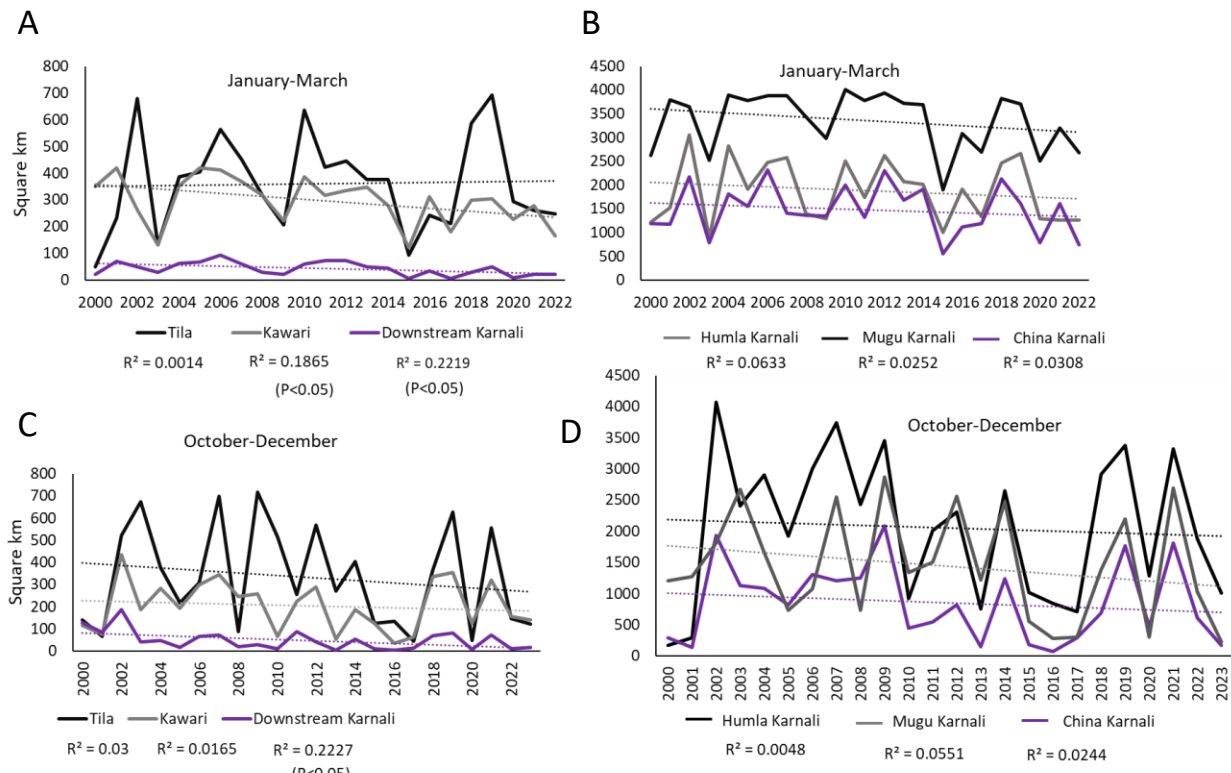
Table 2. Descriptive statistics of snow cover across sub-basins for two seasons (January-March and October-December) and the time series correlation from 2002 to 2024.

Descriptor	January - March						October-December					
	Humla Karnali (China)	Humla Karnali	Mugu Karnali	Tila	Kaweri Down stream	Seasonal average	Humla Karnali (China)	Mugu Karnali	Tila	Kaweri Karnali (Down stream)	Seasonal average	
Mean	1478	3336	1864	351	294	41.9	1227	854	2057	1442	332	204
Median	1420	3667	1827	346	308	39	1239	754	2159	1301	288	190
Standard deviation	501	597	645	184	86.2	24	311	622	1163	862	227	112
Coefficient of variation (CoV in %)	33.90	17.90	34.60	52.42	29.32	57.28	25.35	72.83	56.54	59.78	68.3 7	54.90
Minimum	552	1904	887	50.1	121	5.74	612	67.2	166	226	44.3	35.2
Maximum	2317	4009	3056	691	420	93.5	1642	2092	4074	2868	716	434
Skewness	-0.707	-0.488	-1.29	-0.69	-0.469	-0.763	-1.1	0.533	-0.016	0.231 7	0.34 7	185
Temporal correlation (r<0.44 and r>0.44, p<0.05	-0.16	-0.18	-0.10	0.12	-0.37	-0.41	-0.14	-0.16	-0.07	-0.23 -0.17	0.17 -0.13	-0.47 -0.17

374

375

376



377

378 **Figure 6.** The snow cover trend in the Upper Karnali Basin varies across different sub-basins
 379 from January–March and from October–December (A-D).

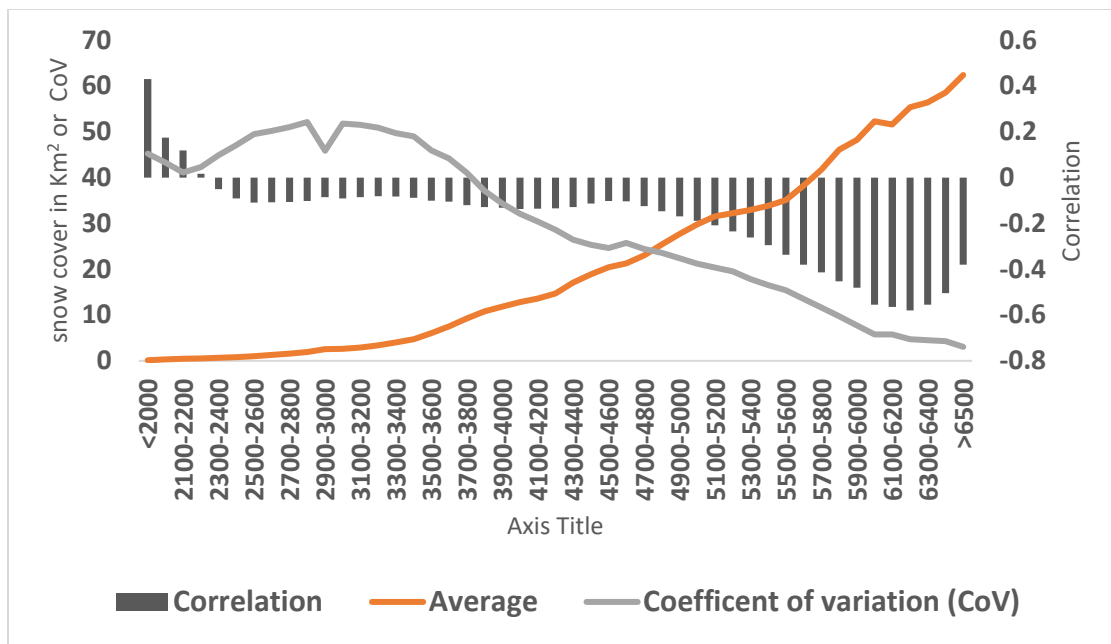
380 4.4. Snow Cover Dynamics across Elevation Zones

381 The dynamics of snow cover across elevation zones, categorized in 100-meter intervals from
 382 ≤ 2000 m to ≥ 6500 m, reveal remarkable elevation-dependent patterns in correlation and
 383 variability (Figure 7) with time (2002-2024). Snow cover in the lowest elevation zones shows a
 384 weak positive correlation (0.12-0.43), suggesting a marginal increase. However, pronounced

385 interannual variability (CoV ~ 41-43%) is likely driven by fluctuating temperature and
386 precipitation regimes (Pendergrass, 2020).

387 Above 2300 m a.s.l., correlations shift to weak negative values (up to 5000 m a.s.l., $r = -0.05$ to -
388 0.17, reaching peak negativity at 6100-6200 m a.s.l. ($r = -0.56$), indicating a significant decline in
389 snow cover (Figure 7). This trend aligns with the impacts of global warming, where rising
390 temperatures disproportionately affect higher elevations, accelerating snowmelt and reducing
391 accumulation (Naegeli et al., 2019; Ren et al., 2023; Shen et al., 2021). The mean snow cover
392 increases with elevation, showing a marked rise from 3300 to 6500 m a.s.l. or above, except
393 between 5000-5200 m a.s.l, which exhibits a gradual rise in snow cover.

394 Above this elevation, the mean snow cover area rises sharply, coinciding with glaciers and
395 permanent snow zones. In contrast, the CoV increases with elevation up to 3100 m a.s.l. and then
396 trends sharply downward from 3100 m a.s.l. to 6500 m a.s.l. and beyond. This pattern indicates a
397 decline in interannual variability alongside increased negative correlations. The low inter-
398 variability reinforces the reliability of the declining trend in snow cover.

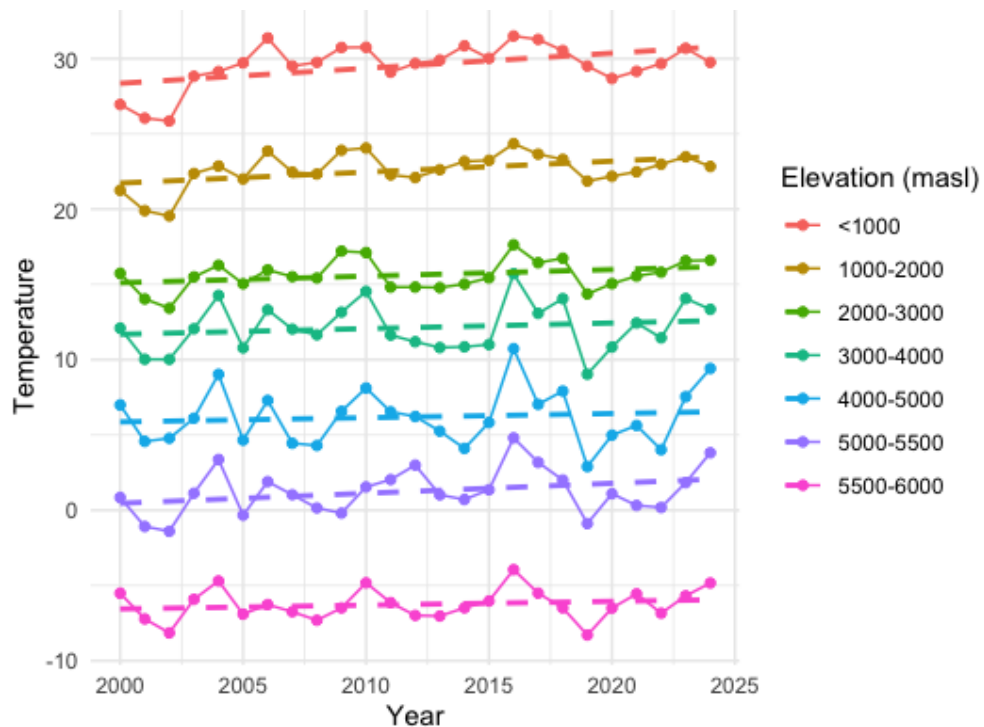


399

400 **Figure 7.** The average, coefficient of variation, and correlation of snow cover area (Source :
 401 MODIS) across various elevation bands **with time (2002-2024).**

402 To examine the relation between temperature and snow cover, the elevation bands were
 403 regrouped into seven broader bands: <1000, 1000–2000, 2000–3000, 3000–4000, 4000–5000,
 404 5000–5500, 5500–6000, and above 6000 m a.s.l. The temperature trend from 2002 to 2024
 405 across elevation bands in the Upper Karnali Basin, as evidenced by Sen's slope (Figure 8, Table
 406 3), shows a general increase. The highest rate of change is observed at lower elevations (<1000
 407 m: 0.0765°C/year). Mid-elevations (1000-2000m: 0.0576°C/year) and high elevations (5000–
 408 5500 m: 0.0643°C/year) also **exhibit significant** warming. However, statistical significance (P-
 409 value) weakens at higher elevations. This warming accelerates glacier retreat, reducing snow
 410 cover and impacting the **hydrology of the Upper Karnali Basin by altering river flow**
 411 **patterns and** leading to a declining glacier-fed water supply.

412



413

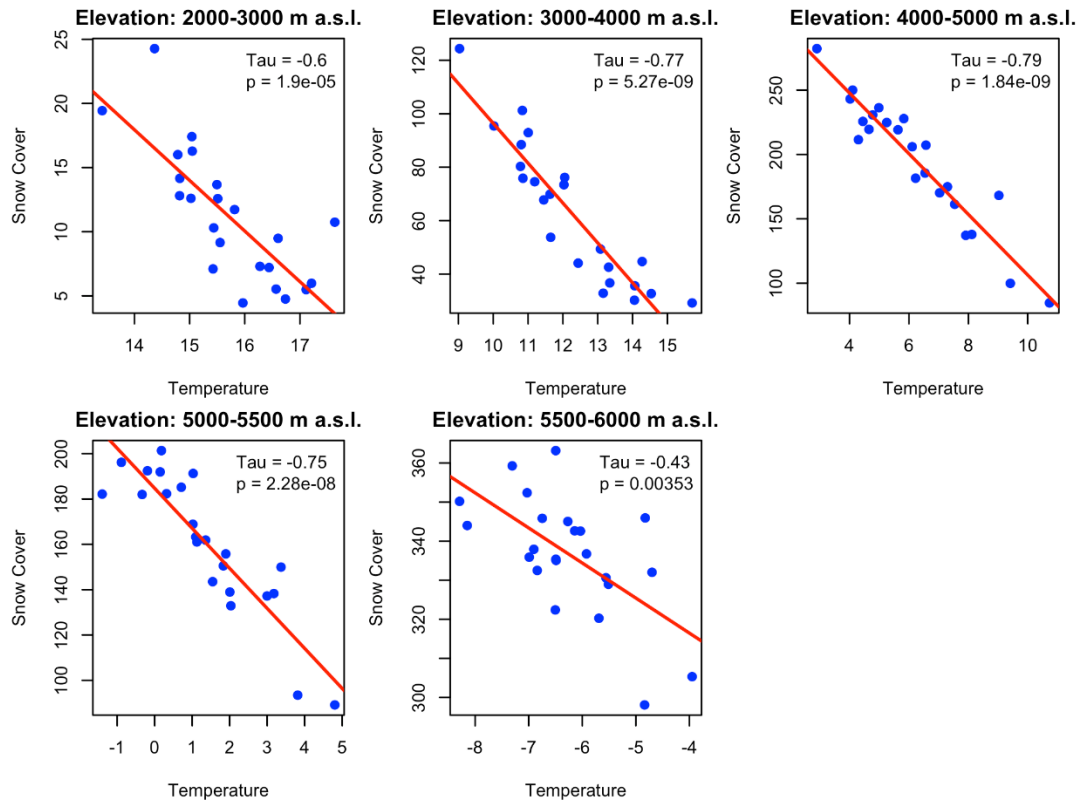
414 **Figure 8.** Temperature (source: MODIS) trend between 2002 and 2024 for different elevation
415 bands

416

418 **Table 3.** Rate of temperature change in different elevation between 2000–2024)

Elevation bands (m a.s.l.)	Sen's slope(Sen, 1968)	P Value
<1000	0.0765	0.052
1000–2000	0.0576	0.058
2000–3000	0.0390	0.168
3000–4000	0.0410	0.528
4000–5000	0.0198	0.833
5000–5500	0.0643	0.154
5500–6000	0.0287	0.414

419 Figure 9 shows a strong negative correlation between land surface temperature and snow cover
 420 across elevation bands in the Upper Karnali Basin. Tau values range from -0.43 to -0.79. The
 421 correlation is strongest between 3000–5000 m a.s.l. (Tau = -0.77 to -0.79) and 5000–5500 m
 422 a.s.l. (Tau = -0.75), with all p-values <0.01, confirming statistical significance. Even at 5500–
 423 6000 m a.s.l. (Tau = -0.43, p = 0.00353), snow cover continues to decline. **The impact is most**
 424 **severe at mid-to-high elevations, where warming accelerates snowmelt and glacier retreat,**
 425 **highlighting the vulnerability of the Upper Karnali Basin's hydrological balance to climate**
 426 **change.**



427

428 **Figure 9.** Relationship between snow cover and temperature ($^{\circ}\text{C}$) across elevation zones in the
 429 Upper Karnali Basin (2002–2024). The correlation (Kendall's Tau) shows a strong negative
 430 association across all elevations, especially between 3000–5500 m a.s.l., where warming has
 431 significantly reduced snow cover.

432 **Note:** Elevation bands below 2000 m are excluded due to minimal snow presence, high
 433 interannual variability, and limited data reliability.

434 4.5. Snow Cover Trend in Glacier Basins (Landsat Data).

435 We examined using Landsat data snow cover trends in 735 glacier basins, each containing at
 436 least one glacier in 2000 that was greater than 10 hectares, which are crucial for assessing glacial
 437 status, water security, and climate change impacts (Table 4). The minimum altitude of the glacier
 438 basin where all tributary glaciers meet was considered the outlet of the glacier basin. **In these**
 439 **basins, snowfall restocks ice lost to melting, contributing to glacier stability.** Reduced snow

440 cover in the glacier basins accelerates negative mass balance, leading to glacier retreat. These
441 glacier basins are at a minimum altitude above 4000 m a.s.l. with an average of ~5100 m a.s.l.
442 Twenty-five and 75 % lie below 4800 and 5330 m a.s.l., respectively. Besides other
443 meteorological parameters, current temperature trends and albedo patterns play a critical role in
444 glacier mass balance (Dowson et al., 2020; Ye & Tian, 2022). Higher temperatures directly
445 increase the snow melting rate, and a decrease in reflectivity of solar radiation leads to more
446 solar radiation being absorbed by the glacier surface, leading to accelerated melting. Declining
447 permanent snow cover in the glacier basin disrupts the glacier mass balance, affecting glacier
448 persistence, altering water availability, and accentuating climate-driven environmental changes.

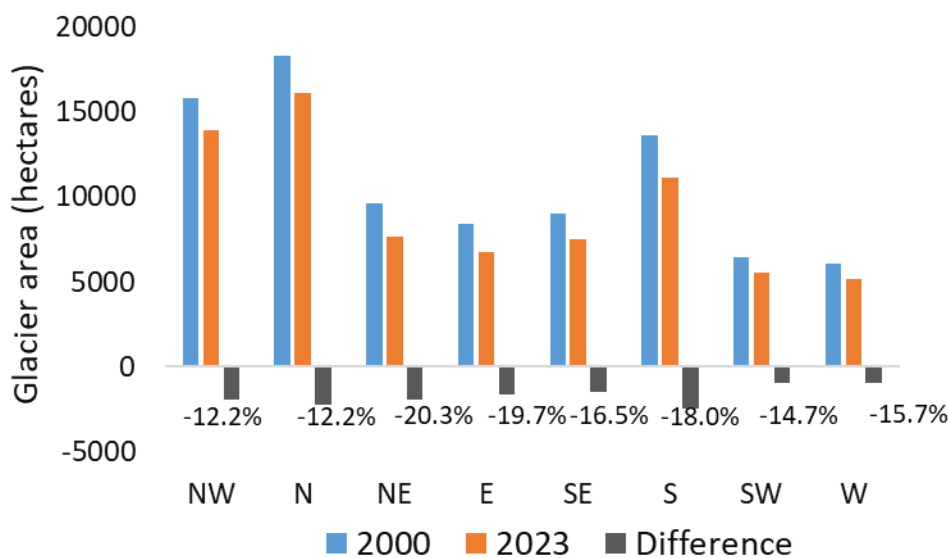
449 The data reveal a significant decline in glacier area across 735 glacier basins between 2000 and
450 2023. The mean glacier area decreased from **119.0 ha in 2000 to 100.5 ha** in 2023, reflecting an
451 average loss of **18.6 ha per basin**. The total glacier area shrank by **13,633.2 ha**, indicating
452 widespread glacier retreat. The percent of glacier area to total basin area declined from 53.23%
453 in 2000 to 44.93% in 2023. Statistical tests show high skewness (>3.9), suggesting that a few
454 large glaciers dominate the dataset. The Shapiro-Wilk test ($p < .001$) confirms a non-normal
455 distribution.

456 **Table 4.** Change in glacier area between 2000 and 2023.

Glacier basin count (N=735)	Glacier basin Area (hectares)	Glacier area (hectares)		Difference in glacier area (hectares)
		2000	2023	
Median	101.4	52.8	39.7	-10.0
Mean	223.6	119.0	100.5	-18.6
Std. Dev	368.1	187.1	169.9	27.2

Skewness	4.6	4.0	4.0	-4.0
Sum	164140.9	87379.9	73746.8	-13633.2

457 The glacier area has declined significantly across all basin directions from 2000 to 2023, with the
 458 basins oriented toward North, Northwest, and Northeast experiencing the largest losses, totaling
 459 6,126.9 hectares (Figure 10). The glaciers oriented towards North-east, East, and South slopes
 460 show the highest relative loss (%). The consistent loss across all directions highlights the
 461 ongoing effects of climate change on the region's glacier-fed water resources.



462

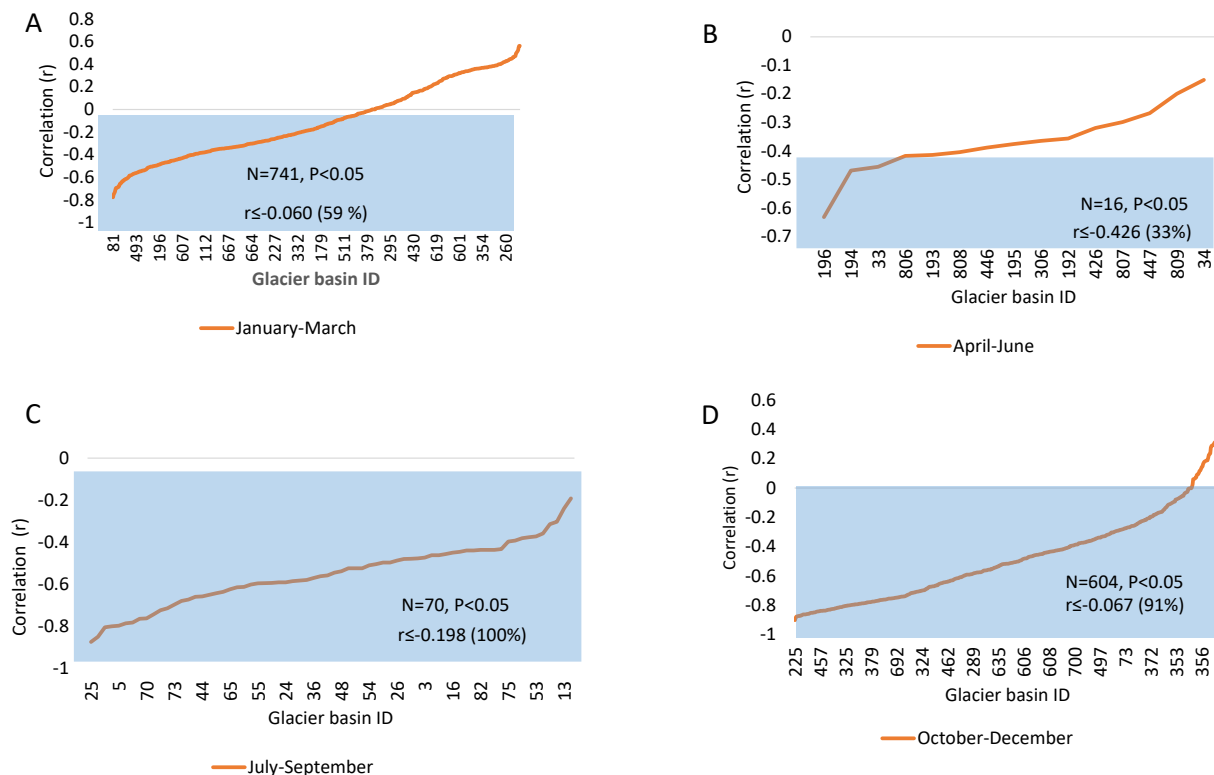
463 **Figure 10.** Change in glacier area in glacier basins by directions between 2000 and 2023.

464 Analysis of snow cover trends indicates that around 59% of glacier basins (n=735) demonstrate
 465 statistically significant negative correlations ($p<0.05$) from January to March. Among these,
 466 glacier basins with a correlation (r) value less than -0.44 represent 16.3% of the total (Figure 11,
 467 12, and 13). Basins with moderate negative correlations, ranging from -0.44 to -0.30, constitute
 468 approximately 19% of the overall total. Additionally, 36% of basins show a positive correlation,

469 with 3% being statistically significant and 13% displaying a moderate correlation. The numerous
 470 glacier basins that exhibit negative correlations suggest a broader regional trend of declining
 471 snow cover over time during winter (January to March).

472 Similarly, during May–July, all 15 cloud-free glacier basins demonstrate a declining trend in snow
 473 cover from 2002 to 2024. Twelve of these basins exhibit a moderate negative correlation ($r < -$
 474 0.30). The trend in snow cover during July–September and October–December also indicates a
 475 decline. **Sixty two percent of the 70 glacier basins show a statistically significant negative**
 476 **correlation ($p < 0.05$)**

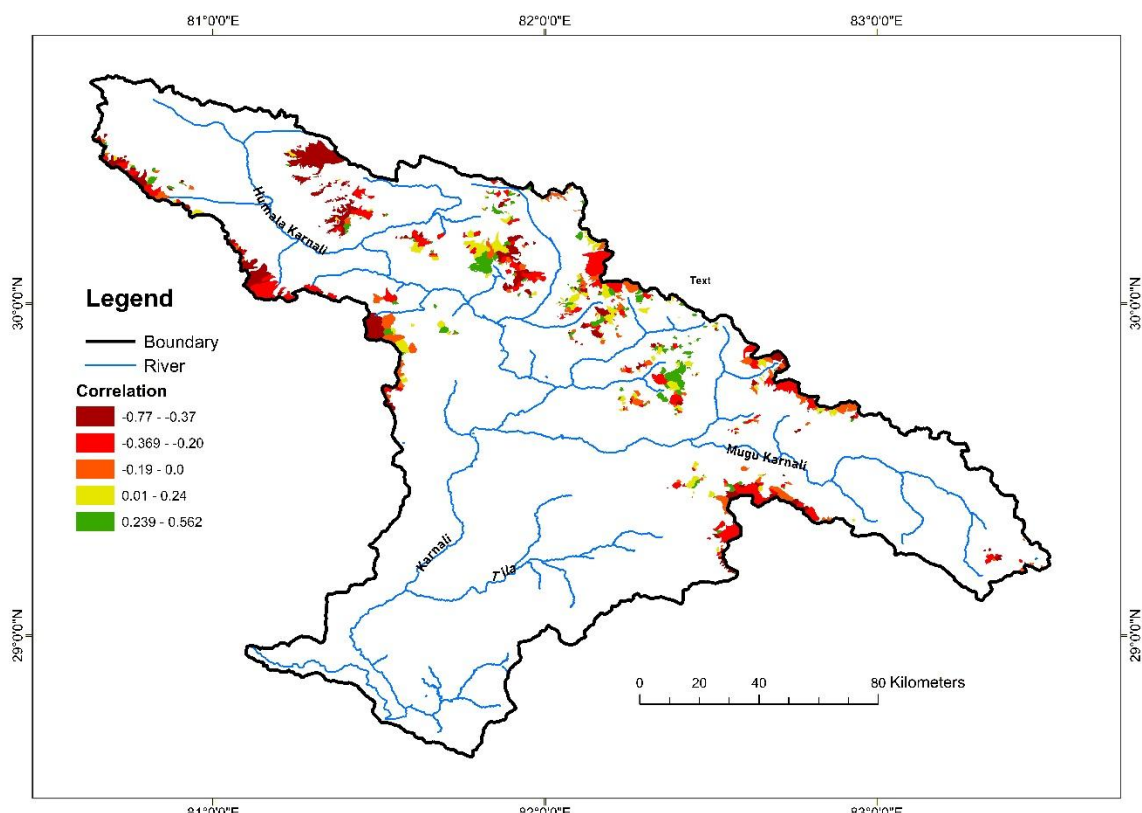
477



478

479 **Figure 11.** The correlation showing the snow cover change between 2002 and 2024 in different
480 glacier basins.

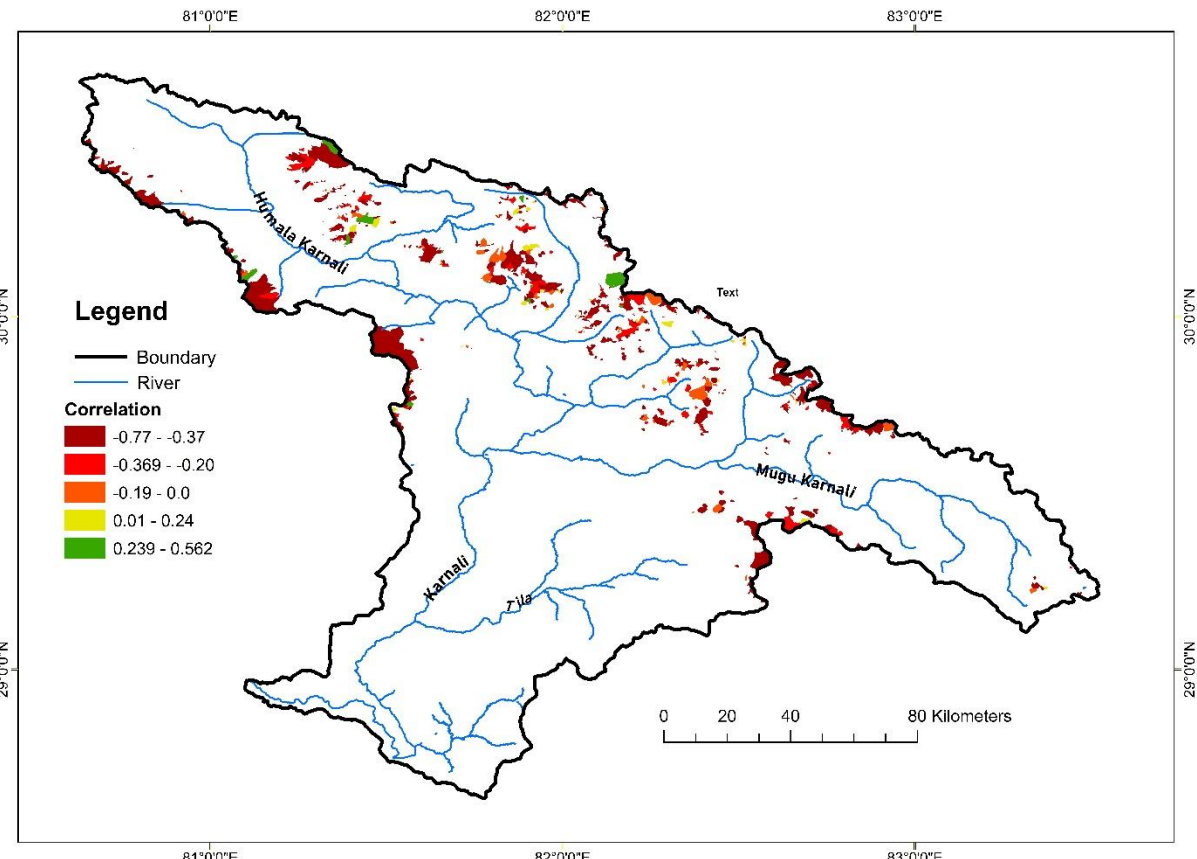
481 The snow cover trend between July–September and October–December for 22 years also
482 demonstrated a consistent decline in all glacier basins. Out of 604 basins selected for the
483 analysis, **about 91%** have shown a statistically significant negative correlation ($p < 0.05$), and 15
484 % of glacier basins showed a moderate negative correlation, i.e., $r = -0.47$ to -0.30 (Figure 10).
485 The snow cover in the remaining basins exhibits a poor negative correlation yet indicates a
486 decline in snow cover over the period.



487
488 **Figure 12.** Snow cover trend on the Glacier Basins for January–March between 2000–2023
489 (Landsat 5, 7, and 8).

490

491



492

493 **Figure 13.** Snow cover trend on the glacier basins for October–December between 2000–2023
494 (Landsat 5, 7, and 8).

495 **4.6. Snowline Shift across Elevations**

496 **Snow-covered areas were derived from the Landsat series 7, 8, and 9 by classifying snow**
497 **using the Normalized Difference Snow Index (NDSI) algorithm to analyze changes in the**
498 **snowline. This analysis was performed on the Google Earth Engine (GEE) platform. Snow pixels**
499 **were identified with an NDSI threshold of > 0.4. The elevation-wise distribution of snow pixels**

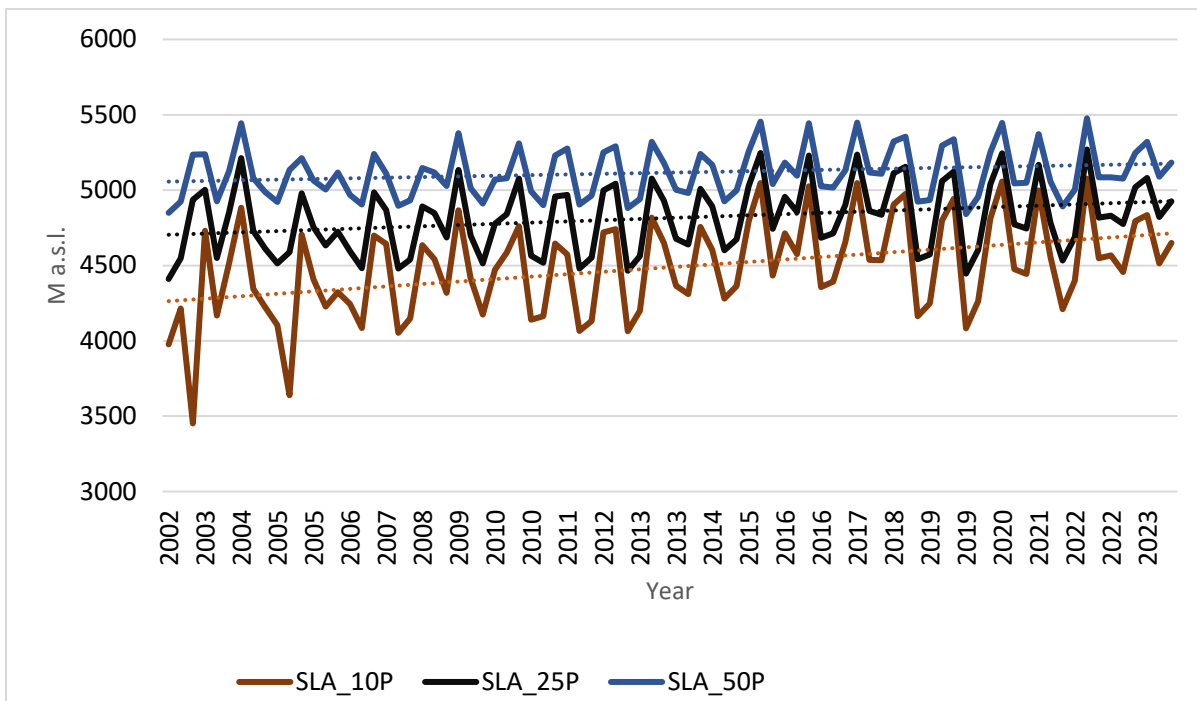
500 was then calculated. To determine the snowline's minimum elevation and its shift from 2002 to
501 2024, three statistical thresholds were applied: the 10th, 25th, and 50th percentiles of the snow
502 cover distribution across various elevations.

503 The analysis of snowline altitude data from 2002 to 2024 reveals a significant upward trend
504 across all percentiles (Figure 14). The 10th percentile shows the largest increase, with a
505 Kendall's tau of 0.2662 and a Sen's slope of approximately 5.16 m/year, indicating that the
506 lower snowline is rising quickly (Table 5). The 25th percentile presents a moderate yet
507 statistically significant trend, with a Kendall's tau of 0.1938 and a Sen's slope of about 2.91
508 m/year. In contrast, the 50th percentile displays a gentler trend, with a Kendall's tau of 0.1483
509 and a Sen's slope of around 1.54 m/yr, which remains statistically significant ($p < 0.05$).
510 Collectively, these findings suggest that the snowline is moving to higher elevations, reflecting
511 broader climatic changes that affect lower elevations more intensively than the median snowline
512 altitude.

513 **Table 5.** Statistical analysis of snow line altitude trends using Kendall's Tau and Sen's slope.

Snow Line Percentile	Kendall's Tau	p-value	Sen's Slope (m/year)	Significance
10th Percentile (SLA_10P)	0.2662	0.00042	5.16	Significant ($p < 0.001$)
25th Percentile (SLA_25P)	0.1938	0.01022	2.91	Significant ($p < 0.05$)
50th Percentile (SLA_50P)	0.1483	0.04942	1.54	Significant ($p < 0.05$)

514



515

516

517 **Figure 14.** Snowline shift using snow line of elevation of 10, 25 and 50 percentile

518 **5.0. Discussions**

519 **This study offers important** insights into the interactions between snow and ice cover in the
 520 Upper Karnali Basin (UKB) and climatic and topographic factors. The results reveal notable
 521 trends and fluctuations in snow cover, glacial retreat, and the elevation of the snowline, aligning
 522 with the wider patterns of climate change seen in the Himalayan region. We will discuss the key
 523 findings below in relation to existing literature and their impact on water resources, ecosystems,
 524 and local communities.

525 The study on the Upper Karnali Basin from 2002 to 2024 reveals significant insights into the
 526 relationship between snow cover area (SCA), temperature, and precipitation. The annual average
 527 SCA is 872 km^2 , with the highest snow cover occurring from January to March ($1528 \pm 333 \text{ km}^2$)

528 and the lowest from July to September ($169 \pm 38.3 \text{ km}^2$). The findings reveal a gradual decline in
529 snow cover across the Upper Karnali Basin (UKB) from 2002 to 2024, with an average loss of
530 $\sim 3.99 \text{ km}^2/\text{year}$.

531 There is a strong to moderate negative correlation between snow cover and temperature across
532 all seasons ($r = -0.59$ to -0.77 , $p < 0.05$), signifying that higher temperatures lead to reduced
533 snow cover. In contrast, precipitation exhibits a positive correlation with snow cover in winter
534 (January to March and October to December). The reduction in snow cover during winter
535 months (January–March) indicates a potential shift in precipitation patterns, with more falling as
536 rain instead of snow. **The winter and pre-monsoon snowpack in the western Himalayas is**
537 **heavily influenced by the Westerly wind system, which is a key source of snowfall in the**
538 **UKB (Syed et al., 2006; Dimri & Dash, 2012). Consequently, the decline in winter snow**
539 **cover may be due not only to temperature-induced changes in precipitation but also to a**
540 **possible weakening or changing of the Westerlies, which needs to be further investigated.**
541 **Such changes could lead to a decrease in overall moisture inflow (Yadav et al., 2009).**

542 This shift is temperature-dependent and thus elevation-dependent, resulting in increased
543 snowmelt, aligning with global warming trends (Wester et al., 2019). During the summer months
544 (April to September), however, precipitation negatively correlates with snow cover, falling
545 predominantly as rain, thus further enhancing snowmelt. Particularly, the period from July to
546 September reveals a statistically significant decrease in snow cover (Sen's Slope = -2.87 ,
547 $p < 0.05$), primarily driven by warmer temperatures and higher rainfall during the summer
548 monsoon, accelerating snowmelt.

549 Examining snow cover patterns in the UKB sub basins reveals notable seasonal and spatial
550 differences. The Humla Karnali sub basin has the largest average snow cover during January–
551 March, while downstream areas like Tila and Kawari **exhibit less snow cover**.
552 The interannual variability in snow cover highlights the sensitivity of snowpack to changing
553 temperature and precipitation patterns. This variability significantly impacts water availability, as
554 the observed reduction in snow cover could worsen water scarcity during the dry season,
555 affecting millions who depend on snowmelt for irrigation, drinking water, **and hydropower**
556 **generation** (Immerzeel et al., 2020; Pritchard, 2019). The strong negative correlation in
557 Downstream Karnali ($r = -0.47$, $p < 0.05$) reinforces the declining trend in snow cover, which
558 threatens water availability and ecosystem services in the region (Wester et al., 2019).
559 The outcomes emphasize the vulnerability of the UKB to climate change, with rising
560 temperatures and shifting precipitation patterns leading to reduced snow cover. Adaptive water
561 management strategies are essential to mitigate the impacts on water resources and local
562 communities.
563 The findings on snow cover dynamics across elevation zones in the Upper Karnali Basin reveal
564 significant elevation-dependent patterns, reflecting the influence of temperature fluctuations and
565 global warming. At lower elevations (≤ 2000 m a.s.l.), snow cover exhibits a weak positive
566 correlation (0.12–0.43), **likely caused by occasional snowfall during short cold spells and a**
567 **shift between rain and snow (Pendergrass, 2020)**. These zones experience high year-to-year
568 **variability (CoV ~41–43%), making trends less reliable, which should be interpreted with**
569 **caution. Similar elevation-sensitive variability has also been reported in other Himalayan**
570 **basins (Pepin et al., 2015)**.

571 The transition from weak negative correlations (**snow cover by elevation and year**) above 2300
572 m a.s.l. to the strongest negative correlation at 6100–6200 m a.s.l. ($r = -0.56$) corresponds with
573 evidence of elevation-dependent warming (EDW), where higher altitudes experience accelerated
574 warming, leading to reduced snow accumulation and increased melt rates. The sharp rise in mean
575 snow cover above 5000 m a.s.l. coincides with permanent snow and glacier zones, but the
576 decline in inter-annual variability (CoV) suggests a consistent reduction in snow cover,
577 particularly at mid-to-high elevations (3000–5000 m a.s.l.).

578 The nonlinear relationship between elevation and inter-annual snow cover variability (CoV)
579 proves particularly insightful. At 3000 m a.s.l. or below, the CoV reaches 41–43%, reflecting
580 transitional zones where slight temperature fluctuations determine the precipitation phase (rain
581 vs. snow). Above 3,000 m a.s.l., CoV drops to 25–30% as conditions remain persistently below
582 freezing, but the dominant driver shifts to insolation and temperature-modulated melt rates. This
583 aligns with Ren et al.'s (2023) findings on Tibetan Plateau glaciers, where albedo feedbacks
584 dominate mass balance above 5000 m a.s.l.

585 The strong negative correlation between land surface temperature and snow cover ($Tau = -0.43$
586 to -0.79) highlights the impact of rising temperatures on snowpack. The most severe declines
587 occur between 3000–5000 m a.s.l., where warming accelerates snowmelt and glacier retreat,
588 threatening water availability for river flows, agriculture, and hydropower (**Immerzeel et al.,**
589 **2020; Bolch et al., 2012**).

590 **Between 2000 and 2023, glacier basins in the Upper Karnali Basin experienced significant**
591 **ice and snow loss. The mean glacier area per basin declined from 119.04 to 100.47 hectares**
592 **with an average loss of 18.6 hectares. While retreat was consistent across all aspects, north-**
593 **facing basins (N, NW, NE) saw the largest total area decline. This trend, driven by rising**

594 **temperatures and reduced snowfall that create a negative mass balance (Pepin et al., 2022;**
595 **Ren et al., 2024; Ye & Tian, 2022), threatens the persistence of glaciers and alters critical**
596 **water resources.**

597 Snow cover trends in glacier basins reveal a consistent decline across all seasons. **From January**
598 **to March, a majority (59%) of the 735 basins analyzed exhibit a statistically significant**
599 **negative correlation ($p < 0.05$), with 16.3% of all basins showing a strong decline ($r < -0.44$).**
600 **The trend is even more pronounced in the post-monsoon and ablation seasons (October–**
601 **December). From July to September, 62% of basins (n=70) show a significant negative**
602 **correlation, and in October–December, this figure rises to 91% (n=604). This widespread**
603 **reduction in snow cover is linked to rising temperatures, which increase snowmelt rates**
604 **and reduce albedo, further accelerating glacier retreat (Dowson et al., 2020). These trends**
605 **underscore the vulnerability of the region's cryosphere to climate change, with serious**
606 **implications for water security and regional hydrology.**

607 **The snowline in the Upper Karnali Basin is rising steadily, with rates of 5.6 m per year**
608 **(10th percentile), 2.91 m per year (25th), and 1.54 m per year (50th). Although these are**
609 **more conservative than many regional estimates, our findings align with the broader**
610 **Himalayan trend of snowline elevation. Recent research reports faster increases, such as**
611 **approximately 6.7–7.3 m per year in the Ganga–Brahmaputra basins (Dixit et al., 2024)**
612 **and roughly 8–14 m per year in several Nepalese catchments (Sasaki et al., 2024), while the**
613 **Langtang Basin shows a similar increase of about 2.2 m per year (Pradhananga et al.,**
614 **2025). This suggests a consistent retreat of seasonal snow cover to higher elevations, which**
615 **reduces the potential for snow accumulation to sustain glacier mass balance.**

616

617 **5.1. Feedback mechanisms and future projections**

618 **The correlation between temperature and snow cover (τ ranging from -0.43 to -0.79 across**
619 **different elevations) confirms the presence of a reinforcing snow–albedo feedback in the**
620 **Upper Karnali Basin (UKB). Increasing land surface temperatures reduces snow cover,**
621 **lowering surface albedo and increasing shortwave radiation absorption. This process**
622 **causes localized warming of about 0.8 to 1.2 °C, as estimated through Sen’s slope analysis,**
623 **further promoting melting and accelerating the feedback loop. Comparable snow–albedo**
624 **feedback mechanisms have been observed across the central and eastern Himalayas (Kääb**
625 **et al., 2015; Bolch et al., 2019; Bhattacharya et al., 2021; Salerno et al., 2021), underscoring**
626 **the regional consistency of cryospheric amplification.**

627 **In addition to snow cover analysis, glacier change data (Ghimire, 2025) were integrated**
628 **with long-term temperature and precipitation records to assess cryospheric variability.**
629 **Relationships among temperature, snow cover, and glacier extent across elevation bands**
630 **were quantified using Kendall’s τ and Sen’s slope, providing estimates of warming trends**
631 **and snowline responsiveness. Future cryospheric conditions were simulated using a degree-**
632 **day, elevation-band glacio-hydrological model forced with bias-corrected CMIP6 (NEX-**
633 **GDDP) climate projections under the SSP1-2.6 and SSP2-4.5 scenarios, enabling**
634 **projections of glacier and snow cover evolution through 2100 (Ghimire et al., 2025b)**

635 **Above 5,000 m a.s.l., Sen’s slope analysis indicates a mean warming rate of $+0.064$ °C per**
636 **year, comparable to the rates observed at mid-elevations (approximately $+0.058$ °C per**
637 **year between 1,000 and 2,000 m). This elevation-dependent warming accelerates glacier**
638 **thinning and shifts the snow–rain boundary upward, thereby reducing accumulation**
639 **periods and causing earlier melt onset (Ghimire et. al., 2025). Similar warming trends, with**

640 mean annual temperature increases of 0.05–0.07 °C per year and glacier thinning rates of
641 0.3–1.0 m per year since 2000, have been documented in the central Himalayas (Kääb et al.,
642 2015; Bolch et al., 2019).

643 Under low-emission scenarios such as SSP1-2.6, high-altitude temperatures are projected
644 to increase by approximately 1 °C by 2100. Under the moderate SSP2-4.5 scenario,
645 temperature increases could reach 2 °C or more. Consequently, glacier areas are expected
646 to decrease by 47–69%. Snow-covered areas are projected to decline by 19–30%. (Ghimire
647 et al., 2025b). This would transform the basin's hydrology from nival (snowmelt-
648 dominated) to pluvial (rain-dominated), increasing flood risks during monsoons and
649 drought susceptibility in dry seasons.

650 These projections align with other studies of Himalayan basins, which forecast reductions
651 in glacier area of 40–60% by mid-century (Bhattacharya et al., 2021; Salerno et al., 2021;
652 Hock et al., 2019). Comparable amplification mechanisms are also evident in the Andes and
653 Alps, where rapid glacier retreat and albedo-induced warming mirror trends observed in
654 the Himalayas (Rabatel et al., 2013; Vuille et al., 2018; Dussaillant et al., 2019; Beniston &
655 Stoffel, 2014; Zemp et al., 2019; Zekollari et al., 2019).

656 6.0. Conclusions

657 The study of snow and glacier cover dynamics in the Upper Karnali Basin from 2002 to 2024
658 reveals a persistent decline in snow cover, glacier area, and snowline elevation, driven by rising
659 temperatures and altered precipitation patterns.

660 The annual snow-covered area (SCA) has decreased by approximately 3.99 km² per year, with
661 the most significant reductions observed during the July–September monsoon period. The decline

662 in snow cover is statistically correlated with increasing temperatures, demonstrating the impact
663 of climate change on seasonal snow accumulation and melt cycles. The winter snow cover
664 variability suggests changes in snowfall patterns rather than a uniform decrease.

665 Notable seasonal and spatial differences in snow cover patterns are observed in the Sub basins of
666 UKB for two seasons, January–March and October–December. The upstream sub basins
667 experience less inconsistent snowfall than the downstream basins. During October–December,
668 snowfall is inconsistent in all basins, but more inconsistent in particularly China Karnali, Tila
669 and Downstream Karnali.

670 Elevation-dependent trend analysis confirms that snow cover at lower elevations (<2000 m a.s.l.)
671 exhibits high interannual variability, while higher elevations (>3000 m a.s.l.) show a significant
672 long-term decline. The strongest reductions occur between 3000–5000 m a.s.l., where warming
673 accelerates snowmelt and glacier retreat. The observed negative correlation between snow cover
674 and rising temperatures confirms the climate-driven reduction in snowpack, exacerbating the risk
675 of water shortages.

676 The study of glacier basins shows widespread retreat, with the mean glacier area declining from
677 119.05 hectares in 2000 to 100.47 hectares in 2023. Glacier retreat is most pronounced in north-
678 facing basins (N, NW, NE), where melting exceeds accumulation. The continuous decline in
679 snow cover across glacier basins indicates an ongoing negative mass balance, threatening long-
680 term glacier persistence.

681 Additionally, the snow line is gradually shifting upward, with the 10th, 25th, and 50th percentiles
682 rising by approximately 5.16, 2.91, and 1.54 meters per year, respectively, indicating a consistent
683 loss of seasonal snow accumulation.

684 **Given the current warming trends (~0.0643°C/year above 5000 m a.s.l.), the UKB could**
685 **experience a decline of glacier area by 47–69 % and snow-covered area by 19–30 %. This**
686 **would transform the hydrology from snowmelt-dominated (nival) to rainfall-dominated**
687 **(pluvial), increasing the frequency of extreme weather events and altering regional water**
688 **security dynamics. The findings emphasize the need for proactive water resource management,**
689 **improved climate resilience strategies, and continuous monitoring of cryospheric changes to**
690 **mitigate future risks. Policymakers must prioritize adaptation measures, such as improved water**
691 **storage infrastructure and sustainable land-use practices, to ensure long-term water security in**
692 **the Upper Karnali Basin and beyond.**

693 **Author contributions**

694 MG conceptualized the research, designed the methodology, conducted fieldwork, analyzed the
695 data, and drafted the manuscript. DS. and RC assisted in proposal writing, research design,
696 fieldwork, and data analysis. AT, TPPS, KPS, SBG, and SD contributed to procuring remote
697 sensing and climate data. PB and SK were responsible for procuring and updating MODIS data.
698 WY reviewed the manuscript and provided feedback to enhance its quality. NT and JK assisted
699 in GIS analysis. All authors contributed to revising the manuscript and provided input before
700 submission.

701 **Competing Interests**

702 The authors declare that they have no conflict of interest.

703 **Data availability**

704 MODIS, Landsat, Sentinel, ERA5 renalysis climate datasets, and NEX-GDDP data are publicly
705 available.

706 **Acknowledgments**

707 We express our gratitude to the Director of Tribhuvan University's Research Coordination and
708 Development Council (RCDC) for supporting the project titled "State and Dynamics of the
709 Cryosphere of the Upper Karnali Basin, Associated Hazards and Implications for Water
710 Resources and Livelihood" (Project Code TU-NPAR-077/78-ERG-15). This paper is a product
711 of that project. We appreciate the Evaluation and Monitoring Committee of RCDC for their
712 insightful feedback and suggestions, which greatly enhanced the manuscript. We also thank the
713 University Grants Commission for providing research funding. Authors would also like to
714 sincerely acknowledge the Sichuan Science and Technology Program (2024YFHZ0248) for
715 partial support. We also acknowledge the contributions of Google Earth Engine, ERA5, ESRI,
716 and other open-access resources for providing satellite imagery and data.

717 **Financial support**

718 This research was funded by the University Grants Commission (UGC), Kathmandu, through
719 Tribhuvan University's Research Coordination and Development Council (RCDC) under the
720 National Policy Area Research program. The Sichuan Science and Technology Program
721 (2024YFHZ0248) also provided partial funding for this research.

722 **References**

723 Anup, K.: Climate change and its impact on tourism in Nepal, *J. Tour. Hosp. Educ.*, 7, 25–43,
724 <https://doi.org/10.3126/jthe.v7i0.17693>, 2017.

725 **Bajracharya, S. R., Bajracharya, O. R., Baidya, S., Maharjan, S. B., and Shrestha, F.:**
726 **Climate change impact on glaciers in the Langtang and Imja sub-basins of Nepal from late**

727 **70s to 2010, in: AGU Fall Meeting Abstracts, San Francisco, CA, 15–19 December, C31B-**
728 **0278, 2014.**

729 **Beniston, M. and Stoffel, M.: Assessing the impacts of climatic change on mountain water**
730 **resources, Sci. Total Environ., 493, 1129–1137,**
731 **<https://doi.org/10.1016/j.scitotenv.2013.11.122>, 2014.**

732 **Bhattacharya, A., Bolch, T., Mukherjee, K., King, O., Menounos, B., Kapitsa, V., Neckel,**
733 **N., Yao, T., and Li, X.: High Mountain Asian glacier response to climate revealed by multi-**
734 **temporal satellite observations since the 1960s, Nat. Commun., 12, 4133,**
735 **<https://doi.org/10.1038/s41467-021-24180-y>, 2021.**

736 **Bolch, T., Buchroithner, M. F., Kunert, A., and Kamp, U.: Automated delineation of**
737 **debris-covered glaciers based on ASTER data, in: GeoInformation in Europe, edited by:**
738 **Gomarasca, M. A., Millpress, Rotterdam, 403–410, 2007.**

739 **Bolch, T., Kulkarni, A., Kääb, A., Huggel, C., Paul, F., Cogley, J. G., Frey, H., Kargel, J. S.,**
740 **Fujita, K., Scheel, M., Bajracharya, S., and Stoffel, M.: The state and fate of Himalayan glaciers,**
741 **Science, 336, 310–314, <https://doi.org/10.1126/science.1215828>, 2012.**

742 **Bookhagen, B. and Burbank, D. W.: Toward a complete Himalayan hydrological budget:**
743 **Spatiotemporal distribution of snowmelt and rainfall and their impact on river discharge,**
744 **J. Geophys. Res.-Earth Surf., 115, F03019, <https://doi.org/10.1029/2009JF001426>, 2010.**

745 **CBS: National Population and Housing Census 2021 – Province 6 (Karnali) results (online**
746 **tables), Central Bureau of Statistics, Nepal, 2021.**

747 **Desinayak, S., Shrestha, M. S., Gurung, D. R., and Murthy, M. S. R.: Recent changes in**
748 **snow cover extent over the Hindu Kush Himalaya, Int. J. Climatol., 42, 6789–6803,**
749 <https://doi.org/10.1002/joc.7038>, 2022.

750 **Dimri, A. P. and Dash, S. K.: Wintertime climatic trends in the western Himalayas, Clim.**
751 **Change, 111, 775–800, <https://doi.org/10.1007/s10584-011-0201-y>, 2012.**

752 **Dixit, A., Goswami, A., Jain, S., and Das, P.: Assessing snow cover patterns in the Indus–**
753 **Ganga–Brahmaputra River Basins of the Hindu Kush Himalayas using snow persistence**
754 **and snow line as metrics, Environ. Chall., 14, 100834,**
755 <https://doi.org/10.1016/j.envc.2023.100834>, 2024.

756 **Dhital, M. R.: Geology of the Nepal Himalaya: Regional Perspective, Springer**
757 **International Publishing, Cham, Switzerland, 583 pp., <https://doi.org/10.1007/978-3-319-02496-7>, 2015.**

759 Dowson, A. J., Sirguey, P., and Cullen, N. J.: Variability in glacier albedo and links to annual
760 mass balance for the Gardens of Eden and Allah, Southern Alps, New Zealand, The Cryosphere,
761 14, 3425–3448, <https://doi.org/10.5194/tc-14-3425-2020>, 2020.

762 **Duan, S.-B., Li, Z.-L., Li, H., Götsche, F.-M., Wu, H., Zhao, W., Leng, P., Zhang, X., and**
763 **Coll, C.: Validation of Collection 6 MODIS land surface temperature product using in situ**
764 **measurements, Remote Sens. Environ., 225, 16–29,**
765 <https://doi.org/10.1016/j.rse.2019.02.020>, 2019.

766 **Dussaillant, I., Berthier, E., Brun, F., Masiokas, M., Hugonet, R., Favier, V., Rabatel, A.,**
767 **Pitte, P., and Ruiz, L.: Two decades of glacier mass loss along the Andes, Nat. Geosci., 12,**
768 **802–808, <https://doi.org/10.1038/s41561-019-0432-5>, 2019.**

769 Elsasser, H. and Bürki, R.: Climate change as a threat to tourism in the Alps, *Clim. Res.*, 20,
770 253–257, <https://doi.org/10.3354/cr020253>, 2002.

771 Forster, P., Storelvmo, T., Armour, K., Collins, W., Dufresne, J.-L., Frame, D., Lunt, D. J.,
772 Mauritsen, T., Palmer, M. D., Watanabe, M., and Wild, M.: The Earth's Energy Budget, Climate
773 Feedbacks, and Climate Sensitivity, in: *Climate Change 2021: The Physical Science Basis.*
774 Contribution of Working Group I to the Sixth Assessment Report of the Intergovernmental Panel
775 on Climate Change, edited by: Masson-Delmotte, V., Zhai, P., Pirani, A., Connors, S. L., Péan,
776 Berger, S., Caud, N., Chen, Y., Goldfarb, L., Gomis, M. I., Huang, M., Leitzell, K., Lonnoy,
777 E., Matthews, J. B. R., Maycock, T. K., Waterfield, T., Yelekçi, Ö., Yu, R., and Zhou, B.,
778 Cambridge University Press, Cambridge, UK and New York, NY, USA, [923–1054](#),
779 <https://doi.org/10.1017/9781009157896.009>, 2021.

780 **Gafurov, A. and Bárdossy, A.: Cloud removal methodology from MODIS snow cover**
781 **product, *Hydrol. Earth Syst. Sci.*, 13, 1361–1373, <https://doi.org/10.5194/hess-13-1361-2009>,**
782 **2009.**

783 **Gilbert, R. O.: Statistical Methods for Environmental Pollution Monitoring, Van Nostrand**
784 **Reinhold, New York, 272 pp., 1987.**

785 **Gorelick, N., Hancher, M., Dixon, M., Ilyushchenko, S., Thau, D., and Moore, R.: Google**
786 **Earth Engine: Planetary-scale geospatial analysis for everyone, *Remote Sens. Environ.*,**
787 **202, 18–27, <https://doi.org/10.1016/j.rse.2017.06.031>, 2017.**

788 Gurung, D. R., Maharjan, S. B., Shrestha, A. B., Shrestha, M. S., Bajracharya, S. R., and Murthy,
789 M. S. R.: Climate and topographic controls on snow cover dynamics in the Hindu Kush
790 Himalaya, *Int. J. Climatol.*, [37, 3873–3882, https://doi.org/10.1002/joc.5063](#), 2017.

791 Hall, D. K., Riggs, G. A., Salomonson, V. V., DiGirolamo, N. E., and Bayr, K. J.: MODIS snow-
792 cover products, *Remote Sens. Environ.*, 83, 181–194, [https://doi.org/10.1016/S0034-4257\(02\)00095-0](https://doi.org/10.1016/S0034-4257(02)00095-0), 2002.

794 Heid, T. and Kääb, A.: Evaluation of existing image matching methods for deriving glacier
795 surface displacements from repeat optical satellite images, *Remote Sens. Environ.*, 118, 339–
796 355, <https://doi.org/10.1016/j.rse.2011.11.025>, 2012.

797 Hersbach, H., Bell, B., Berrisford, P., Hirahara, S., Horányi, A., Muñoz-Sabater, J., Nicolas, J.,
798 Peubey, C., Radu, R., Schepers, D., Simmons, A., Soci, C., Abdalla, S., Abellán, X., Balsamo,
799 G., Bechtold, P., Biavati, G., Bidlot, J., Bonavita, M., De Chiara, G., Dahlgren, P., Dee, D.,
800 Diamantakis, M., Dragani, R., Flemming, J., Forbes, R., Fuentes, M., Geer, A., Haimberger, L.,
801 Healy, S., Hogan, R. J., Hólm, E., Janisková, M., Keeley, S., Laloyaux, P., Lopez, P., Lupu, C.,
802 Radnoti, G., de Rosnay, P., Rozum, I., Vamborg, F., Villaume, S., and Thépaut, J.-N.: The ERA5
803 global reanalysis, *Q. J. R. Meteorol. Soc.*, 146, 1999–2049, <https://doi.org/10.1002/qj.3803>,
804 2020.

805 **Hock, R., Rasul, G., Adler, C., Cáceres, B., Gruber, S., Hirabayashi, Y., Jackson, M., Kääb, A., Kang, S., Kutuzov, S., Milner, A., Molau, U., Morin, S., Orlove, B., and Steltzer, H.: High Mountain Areas, in: IPCC Special Report on the Ocean and Cryosphere in a Changing Climate, edited by: Pörtner, H.-O., Roberts, D. C., Masson-Delmotte, V., Zhai, P., Tignor, M., Poloczanska, E., Mintenbeck, K., Alegría, A., Nicolai, M., Okem, A., Petzold, J., Rama, B., and Weyer, N. M., Cambridge University Press, Cambridge, UK and New York, NY, USA, 131–202, https://doi.org/10.1017/9781009157964.004**, 2019.

812 Hunt, K. M. R., Turner, A. G., and Schiemann, R. K. H.: Western disturbances: a review,
813 **Weather Clim. Dynam.**, **6**, 43–65, <https://doi.org/10.5194/wcd-6-43-2025>, 2025.

814 Ghimire, M., Pangali Sharma, T. P., Chauhan, R., Gurung, S. B., Devkota, S., Sharma, K.
815 P., Shrestha, D., Wei, Z., and Timalsina, N.: Status and changes in glaciers in the Upper
816 Karnali Basin, West Nepal: Assessing topographic influences on area, fragmentation, and
817 volume, **J. Earth Syst. Sci.**, <https://doi.org/10.1007/s12040-025-02664-5>, 2025a.

818 Ghimire, M., Shrestha, D., Zhao, W., Chauhan, R., Gurung, S. B., Pangali Sharma, T. P.,
819 Sharma, K. P., Tamang, S., Timaisina, N., Devkota, S., Thapa, A., Koirala, S., Bhandari,
820 P., Subedi, B., Lohani, U., Kutu, J., Rana, D., and Yanhong, W.: State and Dynamics of
821 Cryosphere of Upper Karnali Basin, Associated Hazards and Implications to Water
822 Resources and Livelihood, Project Code TU-NPAR-077/78-ERG-15, Tribhuvan University,
823 Research Coordination and Development Council (RCDC), Kathmandu, Nepal, 2025b.

824 Immerzeel, W. W., Lutz, A. F., Andrade, M., Bahl, A., Biemans, H., Bolch, T., Hyde, S.,
825 Brumby, S., Davies, B. J., Elmore, A. C., Emmer, A., Feng, M., Fernández, A., Haritashya, U.,
826 Kargel, J. S., Koppes, M., Kraaijenbrink, P. D. A., Kulkarni, A. V., Mayewski, P. A., Nepaul, S.,
827 Pacheco, P., Pak-sok, J., Poulton, C., Pradhan, S., Rangecroft, S., Smeets, S., Suzuki, T., van der
828 Schriek, T., Vivioli, D., Wada, Y., Xiao, C., Yao, T., and Baillie, J. E. M.: Importance and
829 vulnerability of the world's water towers, **Nature**, **577**, 364–369, <https://doi.org/10.1038/s41586-019-1822-y>, 2020.

831 Kääb, A., Berthier, E., Nuth, C., Gardelle, J., and Arnaud, Y.: Contrasting patterns of early
832 twenty-first-century glacier mass change in the Himalayas, **Nature**, **488**, 495–498,
833 <https://doi.org/10.1038/nature11324>, 2012.

834 Kääb, A., Reynolds, J. M., and Haeberli, W.: Glacier and permafrost hazards in high mountains,
835 in: **Global Change and Mountain Regions**, edited by: Huber, U. M., Bugmann, H. K. M., and
836 Reasoner, M. A., Springer, Dordrecht, 225–234, https://doi.org/10.1007/1-4020-3508-X_23,
837 2005.

838 **Khadka, N., Li, B., Wu, Q., Shrestha, F., Paudel, L., and Wang, W.: Glacial lake outburst**
839 **floods threaten China–Nepal transportation corridors, Sci. Total Environ., 927, 172456,**
840 <https://doi.org/10.1016/j.scitotenv.2024.172456>, 2024.

841 **Khatiwada, K. R., Panthi, J., Shrestha, M. L., and Nepal, S.: Hydro-climatic variability in**
842 **the Karnali River basin of Nepal Himalaya, Climate, 4, 17,**
843 <https://doi.org/10.3390/cli4020017>, 2016.

844 **Krishnan, R., Shrestha, A. B., Ren, G., Rajbhandari, R., Saeed, S., Sanjay, J., Syed, M. A.,**
845 **Vellore, R., Xu, Y., You, Q., and Ren, Y.: Unravelling climate change in the Hindu Kush**
846 **Himalaya: rapid warming in the mountains and increasing extremes, in: The Hindu Kush**
847 **Himalaya Assessment: Mountains, Climate Change, Sustainability and People, edited by:**
848 **Wester, P., Mishra, A., Mukherji, A., and Shrestha, A. B., Springer International**
849 **Publishing, Cham, 57–97,** https://doi.org/10.1007/978-3-319-92288-1_3, 2019.

850 **Kulkarni, A. V., Rathore, B. P., and Singh, S. K.: Distribution of seasonal snow cover in**
851 **central and western Himalaya, Ann. Glaciol., 51, 125–130,**
852 <https://doi.org/10.3189/172756410791386445>, 2010.

853 Kulkarni, A. V., Shirsat, T. S., Kulkarni, A., Negi, H. S., Bahuguna, I. M., and Thamban, M.:
854 State of Himalayan cryosphere and implications for water security, Water Security, 14, 100101,
855 <https://doi.org/10.1016/j.wasec.2021.100101>, 2021.

856 **LRMP: Land Resource Mapping Project (national soils/land-use inventory), Government**
857 **of Nepal, Kathmandu, Nepal, 1986.**

858 **Maskey, S., Thapa, B., and Rijal, K.: Snow cover variability and snowmelt in the**
859 **Himalayan region: A study using MODIS snow products, J. Hydrol. Meteorol., 8, 1–10,**
860 <https://doi.org/10.3126/jhm.v8i1.5920>, 2011b.

861 **Maskey, S., Uhlenbrook, S., and Ojha, S.: An analysis of snow cover changes in the**
862 **Himalayan region using MODIS snow products and in-situ temperature data, Clim.**
863 **Change, 108, 391–400,** <https://doi.org/10.1007/s10584-011-0033-6>, 2011a.

864 Mimura, N.: Sea-level rise caused by climate change and its implications for society, Proc. Jpn.
865 Acad. Ser. B, 89, 281–301, <https://doi.org/10.2183/pjab.89.281>, 2013.

866 Muhammad, S. and Thapa, A.: An improved Terra–Aqua MODIS snow cover and Randolph
867 Glacier Inventory 6.0 combined product (MOYDGL06*) for high-mountain Asia between 2002
868 and 2018, Earth Syst. Sci. Data, 12, 345–356, <https://doi.org/10.5194/essd-12-345-2020>, 2020.

869 Naegeli, K., Huss, M., and Hoelzle, M.: Change detection of bare-ice albedo in the Swiss Alps,
870 The Cryosphere, 13, 397–412, <https://doi.org/10.5194/tc-13-397-2019>, 2019.

871 Nyaupane, G. P. and Chhetri, N.: Vulnerability to climate change of nature-based tourism in the
872 Nepalese Himalayas, Tour. Geogr., 11, 95–119, <https://doi.org/10.1080/14616680802643359>,
873 2009.

874 **Pradhananga, D., Adhikary, S., Dhakal, B. N., Dhakal, A., Ghimire, A., Dhital, S., and**
875 **Manandhar, S.: Cryosphere change in the warming Himalaya: Snow cover and snowline**
876 **trends in Nepal's Langtang Basin (1988–2024), J. Tourism Himalayan Adv., 7, 14–26, 2025.**

877 **Parajka, J. and Blöschl, G.: Spatio-temporal combination of MODIS images – Potential for**
878 **snow cover mapping, Water Resour. Res., 44, W03406,**
879 <https://doi.org/10.1029/2007WR006208>, 2008.

880 **Parris, A. S., Bromirski, P., Burkett, V., Cayan, D. R., Culver, M. E., Hall, J., Horton, R.**
881 **M., Knuuti, K., Moss, R. H., Obeysekera, J., Sallenger, A. H., and Weiss, J. L.: Global Sea**
882 **Level Rise Scenarios for the United States National Climate Assessment, NOAA Tech.**
883 **Memo. OAR CPO-1, 37 pp., 2012.**

884 Pendergrass, A. G.: Changing degree of convective organization as a mechanism for dynamic
885 changes in extreme precipitation, Curr. Clim. Change Rep., 6, 47–54,
886 <https://doi.org/10.1007/s40641-020-00156-z>, 2020.

887 Pepin, N. C., Arnone, E., Gobiet, A., Haslinger, K., Kotlarski, S., Notarnicola, C., Palazzi, E.,
888 Seibert, P., Serafin, S., Stocchi, P., and Zebisch, M.: Climate changes and their elevational
889 patterns in the mountains of the world, Rev. Geophys., 60, e2020RG000730,
890 <https://doi.org/10.1029/2020RG000730>, 2022.

891 Pepin, N., Bradley, R. S., Diaz, H. F., Baraer, M., Caceres, E. B., Forsythe, N., Fowler, H.,
892 Greenwood, G., Hashmi, M. Z., Liu, X. D., Miller, J. R., Ning, L., Ohmura, A., Palazzi, E.,
893 Rangwala, I., Schöner, W., Severskiy, I., Shahgedanova, M., Wang, M. B., Williamson, S. N.,
894 and Yang, D. Q.: Elevation-dependent warming in mountain regions of the world, Nat. Clim.
895 Change, 5, 424–430, <https://doi.org/10.1038/nclimate2563>, 2015.

896 Pfeffer, W. T., Arendt, A. A., Bliss, A., Bolch, T., Cogley, J. G., Gardner, A. S., Hagen, J.-O.,
897 Hock, R., Kaser, G., Kienholz, C., Miles, E. S., Moholdt, G., Mölg, N., Paul, F., Radic, V.,
898 Rastner, P., Raup, B. H., Rich, J., Sharp, M. J., and the Randolph Consortium: The Randolph

899 Glacier Inventory: a globally complete inventory of glaciers, *J. Glaciol.*, 60, 537–552,
900 <https://doi.org/10.3189/2014JoG13J176>, 2014.

901 Pritchard, H. D.: Asia's shrinking glaciers protect large populations from drought stress, *Nature*,
902 569, 649–654, <https://doi.org/10.1038/s41586-019-1240-1>, 2019.

903 Ren, P., Pan, X., Liu, T., Huang, Y., Chen, X., Wang, X., Zhang, Y., and Ling, X.: Glacier
904 changes from 1990 to 2022 in the Aksu River Basin, western Tien Shan, *Remote Sens.*, 16, 1751,
905 <https://doi.org/10.3390/rs16101751>, 2024.

906 Ren, S., Jia, L., Menenti, M., and Zhang, J.: Changes in glacier albedo and the driving factors in
907 the Western Nyainqntanglha Mountains from 2001 to 2020, *J. Glaciol.*, 69, 1500–1514,
908 <https://doi.org/10.1017/jog.2023.33>, 2023.

909 **Rittger, K., Painter, T. H., and Dozier, J.: Assessment of methods for mapping snow cover
910 from MODIS, *Adv. Water Resour.*, 51, 367–380,**
911 <https://doi.org/10.1016/j.advwatres.2012.03.002>, 2013.

912 **Salerno, F., Uccelli, A., Cristofanelli, P., Stocchi, P., Diolaiuti, G., Ma, Y., and Putero, D.:
913 Local cooling and drying induced by Himalayan glaciers, *Nat. Geosci.*, 16, 1120–1127,**
914 <https://doi.org/10.1038/s41561-023-01331-y>, 2023.

915 **Sasaki, O., Miles, E. S., Pellicciotti, F., Sakai, A., and Fujita, K.: Contrasting patterns of
916 change in snowline altitude across five Himalayan catchments, *EGUspHERE* [preprint],**
917 <https://doi.org/10.5194/egusphere-2024-2026>, 2024.

918 **Sen, P. K.: Estimates of the regression coefficient based on Kendall's tau, *J. Am. Stat.
919 Assoc.*, 63, 1379–1389, <https://doi.org/10.1080/01621459.1968.10480934>, 1968.**

920 Shen, L., Zhang, Y., Ullah, S., Pepin, N., and Ma, Q.: Changes in snow depth under elevation-
921 dependent warming over the Tibetan Plateau, *Atmos. Sci. Lett.*, 22, e1041,
922 <https://doi.org/10.1002/asl.1041>, 2021.

923 **Shrestha, M., Wang, L., Koike, T., Xue, Y., and Hirabayashi, Y.: Modeling the spatial**
924 **distribution of snow cover in the Dudhkoshi region of the Nepal Himalayas, J.**
925 **Hydrometeorol.**, 13, 204–222, <https://doi.org/10.1175/JHM-D-10-05005.1>, 2012.

926 **Syed, F. S., Giorgi, F., Pal, J. S., and King, M. P.: Effect of remote forcings on the winter**
927 **precipitation of central southwest Asia part 1: observations, Theor. Appl. Climatol.**, 86,
928 **147–160**, <https://doi.org/10.1007/s00704-005-0217-1>, 2006.

929 **Vuille, M., Carey, M., Huggel, C., Buytaert, W., Rabatel, A., Jacobsen, D., Soruco, A.,**
930 **Villacis, M., Yarleque, C., Elison Timm, O., Condom, T., Salzmann, N., and Sicart, J. E.:**
931 **Rapid decline of snow and ice in the tropical Andes – Impacts, uncertainties and challenges**
932 **ahead, Earth-Sci. Rev.**, 176, 195–213, <https://doi.org/10.1016/j.earscirev.2017.09.019>, 2018.

933 **Wan, Z., Hook, S., and Hulley, G.: MODIS/Aqua Land Surface Temperature/Emissivity**
934 **Daily L3 Global 1km SIN Grid, Version 6, NASA EOSDIS Land Processes DAAC,**
935 <https://doi.org/10.5067/MODIS/MYD11A1.006>, 2015.

936 Wester, P., Mishra, A., Mukherji, A., and Shrestha, A. B. (Eds.): *The Hindu Kush Himalaya*
937 *Assessment: Mountains, Climate Change, Sustainability and People*, Springer Nature, Cham,
938 Switzerland, 627 pp., <https://doi.org/10.1007/978-3-319-92288-1>, 2019.

939 Xu, J., Grumbine, R. E., Shrestha, A., Eriksson, M., Yang, X., Wang, Y., and Wilkes, A.: *The*
940 *melting Himalayas: cascading effects of climate change on water, biodiversity, and livelihoods,*
941 *Conserv. Biol.*, 23, 520–530, <https://doi.org/10.1111/j.1523-1739.2009.01237.x>, 2009.

942 **Yadav, R. K., Rupa Kumar, K., and Rajeevan, M.: Increasing influence of ENSO and**
943 **decreasing influence of AO/NAO in the recent decades over northwest India winter**
944 **precipitation, *J. Geophys. Res.-Atmos.*, 114, D12112, <https://doi.org/10.1029/2008JD011318>,**
945 2009.

946 Ye, Y. and Tian, Y.: Interpreting changes in albedo and mass balance at White Glacier, Canadian
947 Arctic Archipelago, *Int. Arch. Photogramm. Remote Sens. Spat. Inf. Sci.*, XLIII-B3-2022, 793–
948 798, <https://doi.org/10.5194/isprs-archives-XLIII-B3-2022-793-2022>, 2022.

949 **Yu, W., Ma, M., Wang, X., Geng, L., Tan, J., and Shi, J.: Validation of MODIS land**
950 **surface temperature products using ground-based longwave radiation observations in the**
951 **Heihe River Basin, *Proc. SPIE*, 8174, 81741G, <https://doi.org/10.1117/12.898243>**, 2011.

952 **Yue, S. and Wang, C. Y.: The Mann–Kendall test modified by effective sample size to**
953 **detect trend in serially correlated hydrological series, *Water Resour. Manag.*, 18, 201–218,**
954 <https://doi.org/10.1023/B:WARM.0000043140.61082.60>, 2004.

955 **Zemp, M., Huss, M., Thibert, E., Eckert, N., McNabb, R., Huber, J., Barandun, M.,**
956 **Machguth, H., Nussbaumer, S. U., Gärtner-Roer, I., Thomson, L., Paul, F., Maussion, F.,**
957 **Kutuzov, S., and Cogley, J. G.: Global glacier mass changes and their contributions to sea-**
958 **level rise from 1961 to 2016, *Nature*, 568, 382–386, <https://doi.org/10.1038/s41586-019-1071-0>,**
959 2019.

960 **Zemp, M., Roer, I., Kääb, A., Hoelzle, M., Paul, F., and Haeberli, W. (Eds.): Global glacier**
961 **changes: facts and figures, United Nations Environment Programme and World Glacier**
962 **Monitoring Service, Nairobi, Kenya and Zurich, Switzerland, 88 pp., 2008.**

963 Zhao, W., He, J., Wu, Y., Xiong, D., Wen, F., and Li, A.: An analysis of land surface
964 temperature trends in the central Himalayan region based on MODIS products. **Remote**
965 **Sensing**, 11(8), 900.<https://doi.org/10.3390/rs11080900>, 2019.